Earth-Science Reviews 242 (2023) 104459

Contents lists available at ScienceDirect

Earth-Science Reviews

journal homepage: www.elsevier.com/locate/earscirev

A critical review about generic subaerial landslide-tsunami experiments and options for a needed step change

Valentin Heller [a,*], Gioele Ruffini [b]

[a] Environmental Fluid Mechanics and Geoprocesses Research Group, Faculty of Engineering, University of Nottingham, Nottingham NG7 2RD, UK
[b] Department of Civil, Construction and Environmental Engineering, Sapienza University of Rome, Via Eudossiana 18, 00184 Rome, Italy

ARTICLE INFO

Keywords:
Machine learning
Non-linear Fourier transform
Numerical and physical modelling
Subaerial landslide-tsunamis
Tsunamis
Wave energy

ABSTRACT

Subaerial landslide-tsunamis (SLTs) are generated by mass movements such as landslides, rockfalls, glacier calving and snow avalanches impacting into lakes, reservoirs, fjords and the sea. Past SLTs reached runup heights of up to 524 m and are responsible, in combination with associated phenomena and tsunamis generated by partially submerged landslides, for a cumulative death toll in excess of 58000. Generic experimental research into SLTs, i.e. studies intended to predict SLTs for a range of scenarios, is ongoing for many decades. However, the advancement in the physical understanding, the wave prediction accuracy between similar studies and the reliability of hazard assessments does not fully reflect the large number of published generic peer-review work, particularly after 2005. A step change in generic SLT research is therefore needed. This article critically reviews SLT research with a focus on generic empirical equations from laboratory and numerical tests. Key features of past SLT cases are presented, relevant parameters affecting SLTs are reviewed and the most relevant conditions of 76 studies involving 6481 experiments, are listed including 10 milestone studies. This article further reviews findings into the effects of the mass movement type and slide model, slide to wave energy transfer, wave types, the effects of the water body geometry and non-uniform bathymetry, frequency domain analysis, edge waves and analytic achievements. Research gaps and shortcomings around generic empirical equations are also highlighted. Options to contribute to a step change are then suggested. These include the Korteweg-de Vries and Kadomtsev-Petviashvili equations, a generally applicable numerical code, machine learning and combinations.

1. Introduction

1.1. Background

Subaerial landslide-tsunamis (SLTs) are generated by mass movements such as landslides, rockfalls, glacier calving and snow avalanches impacting into water bodies including lakes, reservoirs, fjords and the sea. The term ‘tsunami’ (translated from Japanese as ‘harbour wave’) originally only included waves generated in oceans, with the more general term ‘impulse wave’ used for all types of water bodies. However, ‘tsunami’ is now widely used also for restricted water bodies such as lakes and reservoirs (Kremer et al., 2021) and ‘tsunami’ in this more general meaning will be applied herein also to describe impulse waves. Further, the term ‘landslide’ represents different types of mass movements herein, including rockslides, rockfalls, glacier calving and snow avalanches.

SLTs heights locally often exceed the size of earthquake or meteo tsunamis or of underwater landslide-tsunamis. Some past SLT events were specified as ‘megatsunamis’ with an initial wave height of tens or hundreds of meters. Fortunately, the destructive potential of most SLTs is limited to a local, rather than an ocean wide scale, as they typically origin from a point source. This is different to earthquake tsunamis typically originating from a line source (2004 Indian Ocean tsunami (Jankaew et al., 2008)), decaying slower with propagation distance.

Fig. 1 shows past megatsunamis: (a) the 1958 Lituya Bay SLT with an observed runup height of 524 m (Fritz et al., 2001), (b) the 2014 Lake Askja rockslide case on Iceland with a maximum runup height of 71 m (Gylfadóttir et al., 2017) and (c) the 50 m SLT caused at the Eqip Sermia outlet glacier front in Greenland in 2014 (Lüthi and Vieli, 2016). A larger selection of past subaerial and partially submerged landslide-tsunamis with some key parameters is given in Table 1 and the global catalogue of Roberts et al. (2014) includes 254 SLTs. The cumulative death toll of the cases in Table 1 exceeds 58000 (due to tsunamis and associated phenomena such as volcanic explosions and landslides), and

* Corresponding author.
E-mail addresses: valentin.heller@nottingham.ac.uk (V. Heller), gioele.ruffini@uniroma1.it (G. Ruffini).

https://doi.org/10.1016/j.earscirev.2023.104459
Received 31 December 2021; Received in revised form 17 May 2023; Accepted 23 May 2023
Available online 29 May 2023

they caused severe economic losses e.g. through destroyed infrastructure. SLT research and hazard assessment methods aim to reduce such losses.

Humans have been able to prevent SLTs in rare cases by stabilising creeping landslides, such as at the Clyde Dam reservoir (MacFarlane, 2009), or by removing a part of the landslide (Huang et al., 2023). However, more common than preventing SLTs are mitigation measures to deal with SLTs such as early warning and evacuation, territorial panning, reservoir level drawdown, controlled blasting and the provision of an adequate freeboard when designing a dam (Evers et al., 2019b; Harbitz et al., 2014). Essentially 5 approaches are available to support these measures and to predict SLTs: (I) generic empirical equations from laboratory and numerical tests, (II) prototype-specific physical model tests, (III) protype-specific numerical model tests, (VI) empirical equations derived from field data and (V) analytical investigations (Evers et al., 2019b). These 5 approaches are often combined (e.g. (II) or (III) follows a preliminary assessment based on (I) or (II) is used to validate (III)) and can also feed into a more holistic method such as a probabilistic tsunami hazard and risk analysis (Grezio et al., 2017; Behrens et al., 2021; Iorio et al., 2021).

In approach (I) the governing parameters (slide velocity, volume, geometry, hill slope, water depth, etc.) are systematically varied under idealised conditions and the wave parameters are then expressed through generic empirical equations as a function of these governing parameters. Such generic findings are therefore intended to predict SLTs for a range of scenarios (slide geometries and properties, water body geometries, bathymetries, etc.), in contrast to prototype-specific studies. The application of such equations is inexpensive and efficient, but provides preliminary estimates only, with some uncertainties for complex water body shapes. In the authors personal view and generally speaking, (II) is currently the most reliable approach, but time-consuming and expensive for sufficient large scales to avoid significant scale effects. Approach (III) requires less resources, but high-quality calibration and validation data. Approaches (IV) and (V) are rarer applied in SLT hazard assessment; Approach (IV) is associated with significant uncertainties due to a lack of field measurements and challenges in applying observations from one case to others, and (V), even though in principle able to describe the main features of the phenomenon, typically excludes wave generation and is based on simplified assumptions such as linear wave theory (Noda, 1970; Wiegel et al., 1970; Renzi and Sammarco, 2010; Section 2.11).

Despite a large number of generic research studies, the research progress in SLTs since 2005 is slow and dominated by empirical investigations. Reliable hazard assessment methods are still lacking and the reliable prediction of SLTs remains challenging. Most ongoing research aims to reproduce individual SLT laboratory or field cases numerically (approach III) or to create more empirical equations to add to (I). However, wave parameters predicted with empirical equations based on (I) can vary by 1 to 2 orders of magnitudes even when derived under similar conditions (Fritz et al., 2004; Heller and Hager, 2010; Watt et al., 2012; Heller and Spinneken, 2013, 2015; Evers and Hager, 2016; Bullard et al., 2019a; Section 3.2) and they ignore some key physical principles (e.g. the fact that SLTs are composed of superimposed wave components, frequency dispersion, etc.). On the other hand, method (III) is often successful in reproducing idealised individual cases after a case-specific calibration, but if applied to other, more complex slide scenarios and reservoir geometries and bathymetries, often fails to provide satisfactory predictions (Heller et al., 2016; Rauter et al., 2022).

1.2. Focus, aims and structure

This review article focuses on the generation and propagation of SLTs, mainly based on approach (I): Generic empirical equations from laboratory and numerical tests. This involves the wave parameters offshore of shores and structures, being key inputs for probabilistic tsunami hazard and risk analyses and for studies addressing the effects of SLTs such as runup heights, overland flows, inundation depths, loading

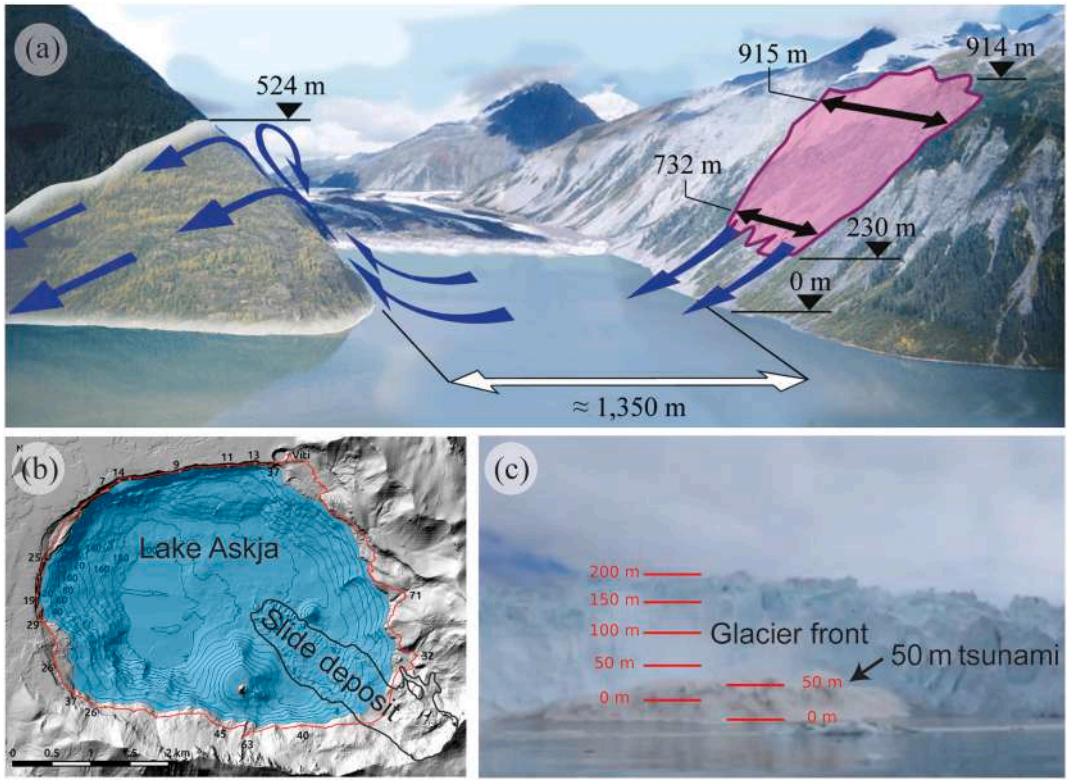

Fig. 1. Past SLTs: (a) 524 m runup observed in the 1958 Lituya Bay case in Alaska (Fritz et al., 2001), (b) 2014 Lake Askja rockslide case on Iceland (Gylfadóttir et al., 2017) and (c) a 50 m wave generated by a calving iceberg at the Eqip Sermia outlet glacier front in Greenland in 2014 (Lüthi and Vieli, 2016).

Table 1
Dates and locations of past subaerial and partially submerged landslide-tsunamis with the composition of the landslide, some relevant parameters (bulk slide volume $\forall_s$, slide impact angle α, still water depth h) and the effects (maximum runup height R and number of fatalities (due to tsunamis and associated phenomena such as volcanic explosions and landslides)).

Date, Location	Composition	Parameters	Effects	Reference
		$\forall_s$ [m^3], α [°], h [m]	R [m], fatalities	
170000 years ago, Tenerife (Canary Islands)	Debris avalanche	$1200–1500 \times 10^6$, -, 500	132, -	Paris et al. (2017)
1740, Oshima-Oshima (Japan)	Rock/debris	2500×10^6, -, 500–1000	≈13, 2000	Satake (2007)
22.02.1756, Tjelle (Norway)	Granite gneiss	15×10^6, >25, >200	46, 38	Slingerland and Voight (1979)
07.02.1784, Scilla (Italy)	Gneiss/breccia	5.4×10^6, 45, 300	≤ 16, 1500	Mazzanti and Bozzano (2011)
21.05.1792, Shimabara (Japan)	Volcanic debris	500×10^6, 10, 64	10, >15000	Slingerland and Voight (1979)
27.08.1883, Krakatau (Indonesia)	Pyroxene/basalt	10000×10^6, -, ≤ 100	42, 36000	Choi et al. (2003)
13.03.1888, Ritter Island (Papua New Guinea)	Basalt/andesite	5000×10^6, 10–15, 1000	15–20, >100	Ward and Day (2003)
04.07.1905, Disenchantment Bay (USA)	Ice	29×10^6, 28, 80	35, 0	Slingerland and Voight (1979)
16.01.1905, Ramnefjellet (Norway)	Schist/debris	3×10^5, -, 15–30	40.5, 61	Waldmann et al. (2021)
07.04.1934, Tafjord (Norway)	Gneiss	$2–3 \times 10^6$, 60, >200	62, 41	Slingerland and Voight (1979)
13.09.1936, Ramnefjellet (Norway)	Gneiss	1×10^6, 25, < 60	74, 73	Slingerland and Voight (1979)
09.07.1958, Lituya Bay (USA)	Schist	31×10^6, 40, 122	524, 2	Slingerland and Voight (1979)
22.03.1959, Pontesei reservoir (Italy)	Silt/clay debris	5×10^6, ≈5, 47	-, 1	Panizzo et al. (2005a)
09.10.1963, Vajont reservoir (Italy)	Limestone	240×10^6, 0–40, 50	270, ≈2000	Slingerland and Voight (1979)
18.03.1971, Yanawayin Lake (Peru)	Limestone	1×10^5, 45, 38	30, 400–600	Slingerland and Voight (1979)
18.07.1979, Lembata (Indonesia)	Volcanic	17×10^6, -, -	< 10, ≈900	Paris (2015)
18.05.1980, Mount St. Helens (USA)	Rock/sediments	430×10^6, 50–60, -	260, 0	Meyer and Carpenter (1983); Voight et al. (1983)
12.06.1985, Xintan, Yangtze River, Three Gorges (China)	Alluvial/colluvial debris	20×10^6, 23, 30–40	49, > 12	Huang et al. (2009)
21.11.2000, Paatuut (Greenland)	Basaltic material	30×10^6, 60, 650	50, 0	Dahl-Jensen et al. (2004)
30.12.2002, Stromboli (Italy)	Volcanic	$4–9 \times 10^6$, -, -	< 11, 0	Tinti et al. (2006)
13.07.2003, Qianjiangping, Three Gorges Reservoir (China)	Rock/gravel/clay	24×10^6, 13–35, 45	39, 24	Yin et al. (2015)
04.12.2007, Chehalis Lake (Canada)	Rock	3×10^6, 30, 120	38, 0	Wang et al. (2015)
20.07.2007, Lake Lucerne (Switzerland)	Rock	8000, 30–70, 146	-, 0	Fuchs and Boes (2010)
13.11.2008, Gongjiafang, Three Gorges Reservoir (China)	Disintegrated rock	3.8×10^5, 44–64, 47	13.1, 0	Huang et al. (2012)
12.01.2010, Grand Goâve (Haiti)	Sediments	-, -, -	3, 3	Fritz et al. (2013)
02.07.2014, Eqip Sermia (Greenland)	Ice	9×10^5, 90, 100–150	15, 0	Lüthi and Vieli (2016)
21.07.2014, Lake Askja (Iceland)	Rock	10×10^6, 10.4, 138	60–80, 0	Gylfadóttir et al. (2017)
17.10.2015, Taan Fjord (Alaska)	Rock	$70–80 \times 10^6$, ≈35, -	150, 0	George et al. (2017)
24.06.2015, Hongyanzi, Three Gorges Reservoir (China)	Sediments	23×10^4, 31, 70	6, 2	Xiao et al. (2018)
17.06.2017, Karrat Fjord (Greenland)	Rock	45×10^6, 50, 100–200	10, 4	Paris et al. (2019)
11.10.2018, Baige, Jinsha River (China)	Rock	15×10^6, 30–50, ≈70	140, 0	Hu et al. (2020)
22.12.2018, Anak Krakatau (Indonesia)	Volcaniclastic	$300–200 \times 10^6$, -, 200	13, 437	Grilli et al. (2019)
28.11.2020, British Columbia (Canada)	Rock/quartz diorite	13×10^6, 8–90, ≈50	114, 0	Geertsema et al. (2022)

and overtopping (Wüthrich et al., 2018; Evers et al., 2019b; Attili et al., 2021). However, these latter effects are not reviewed herein. Further, the focus is on peer-reviewed laboratory and numerical studies for advancing approach (I), rather than on theses, conference proceedings and case studies. Numerical methods and treatments of SLTs are only briefly covered in Section 4.3 and the reader is referred to the extensive review of Yavari-Ramshe and Ataie-Ashtiani (2016) for a more comprehensive overview. Excluded are also uncertainties associated with landslides such as where they occur and their size (Løvholt et al., 2020), i.e. the reviewed SLT approaches mainly apply to unstable landslides and support the design of reservoirs where this information can be estimated.

Further extensive reviews with other foci have been presented by Slingerland and Voight (1979) including both laboratory studies and past cases, Heller et al. (2009) formulating a hazard assessment manual to predict the effects of SLTs in lakes and reservoirs, Di Risio et al. (2011) focusing on empirical equations, Hager and Evers (2020) covering experimental work up to 1990, Romano (2020) including details of experimental and numerical studies of the last 10 years, Kremer et al. (2021) reviewing various types of past freshwater tsunamis and Grezio et al. (2017) and Behrens et al. (2021) reviewing probabilistic tsunami hazard and risk analysis. After presenting a review of SLTs based on generic experiments, a range of promising concepts with the potential to contribute to a needed step change in generic SLT research are suggested.

The remainder of this article is organised as follows: In Section 2 the state of the art of SLT is presented with focus on approach (I). This includes a discussion of the relevant parameters for SLTs (Section 2.2) and a complete list of studies applying approach (I) including 10 milestone studies (Section 2.3). This is followed by summaries of findings into the effects of the mass movement type and slide model (Section 2.4), slide to wave energy transfer (Section 2.5), wave types (Section 2.6), the effects of the water body geometry (Section 2.7) and non-uniform bathymetry (Section 2.8), frequency domain analysis (Section 2.9), edge waves (Section 2.10) and analytic achievements (Section 2.11). Section 3 highlights the gaps and shortcomings in current research approaches with focus on approach (I). Options for a step change are then introduced in Section 4. This includes the Korteweg-de Vries and Kadomtsev-Petviashvili equations (Section 4.2), a generally applicable numerical code (Section 4.3) and machine learning (Section 4.4). Finally, Section 5 highlights the main conclusions of this review article.

2. State of the art

2.1. Introduction

This section provides a state of the art of SLT research with particular focus on approach (I): Generic empirical equations from laboratory and numerical tests. Fig. 2(a) shows a definition sketch of the relevant slide parameters reviewed in Section 2.2. The most relevant SLT parameters

are the maximum (subscript M) wave amplitude a_M, height H_M and period T_M and their evolutions with distance from the slide impact. Note that T_M is typically defined as the period of the wave where a_M was measured, and a_M and H_M can be observed at two different waves, sometimes at the 2nd and/or 3rd wave. Also illustrated in Fig. 2 are the idealised water body geometries commonly applied in approach (I), namely a 2D (prismatic flume, water body side angle $\theta = 0°$, Fig. 2b) and 3D geometry (prismatic basin, $\theta = 90°$, Fig. 2c). In 2D the tsunamis propagate in the x direction with straight wave fronts and the energy is laterally constrained. In 3D, however, the tsunamis vary with the radial distance r and the wave propagation angle γ, with the coordinate origin shown in Fig. 2.

Fig. 3, showing a laboratory experiment, is used to introduce into SLTs. The slide located on the top left in Fig. 3(a) is modelled as a rigid block in this experiment, and its release height, dimensions, density and the slope angle are all relevant parameters affecting the SLTs features (Section 2.2). The 76 generic SLT studies (98 individual publications) in Table 2 were aimed at investigating the effects of these and further parameters on SLTs (Fig. 2).

In Fig. 3(a) the block slide is released and reaches the 0.24 m deep water shortly before the instant shown in Fig. 3(b). The tsunami energy spreads as a function of (r, γ) in this 3D geometry, i.e. along the slide axis and laterally. The slide creates an outward collapsing impact crater in Fig. 3(c) whilst transferring momentum to the water body. This results in a 3-phase (solid, water and air) flow. Only a part of the slide energy is transferred into SLTs whilst the remaining energy is consumed by mechanisms such as basal friction, slide impact on the water body bottom and dissipative processes in the water body (Section 2.5). Pressure sensors located at the slide front (Fig. 3a) reveal that the slide transfers most of its momentum within 0.5 s to the water body for this fast moving slide at laboratory scale.

The impacting slide creates the primary positive elevation (SLTs are always leading elevation for the offshore propagating waves). They propagate radially from the slide impact zone in Fig. 3(d,e) affected by turbulence from the violent wave generation process. The waves are largest on the slide axis $\gamma = 0°$ and decay with increasing/decreasing γ. A wave train is further generated, and the primary wave is not always the largest. The slide runs out continuously along a circular transition at the slope toe before the drag, friction and buoyancy forces overcome the gravity and inertial forces and stop the slide with its front on the right-hand side of the picture in Fig. 3(f). Meanwhile, the primary wave propagates further away from the slide impact zone whilst the impact crater closes and creates an uprush on the hill slope (Fig. 3d,e,f). The following rundown creates another wave behind the primary wave in the wave train. Waves also propagate along the slide impact shore as edge or trapped waves (Fig. 3c,d,e,f) partially governed by different physical processes than the freely offshore propagating waves (Section 2.10). The SLT train propagates then further in the far field on a uniform bathymetry, which can also affect the waves (Section 2.8).

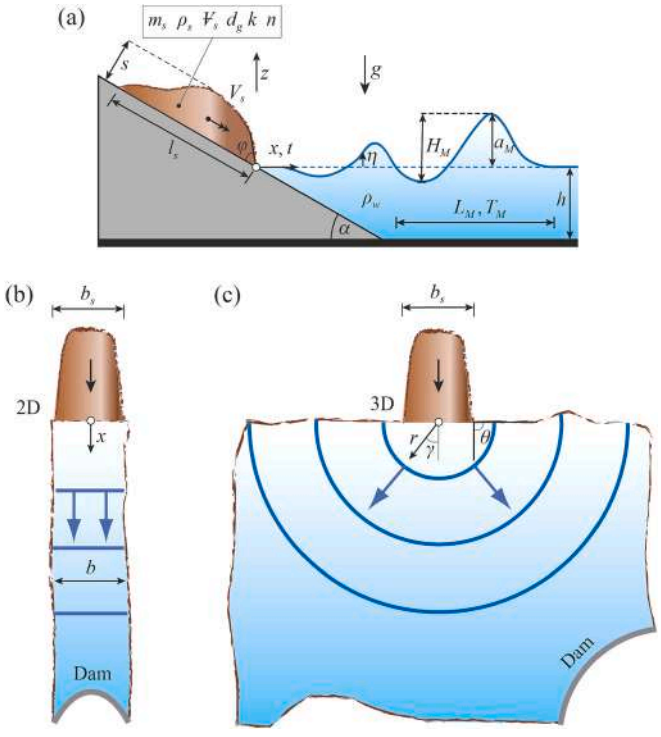

Fig. 2. Definition sketches: (a) side view of slide and SLT with slide and wave parameters, and bird view of a (b) 2D and (c) 3D geometry.

The free water surface is measured over time at fixed locations with wave probes (vertical wires with white splash protections shown in Fig. 3). Fig. 4 shows the time series recorded at $r/h = 3.0$, 7.5, 15.0 and 35.0 along the slide axis ($\gamma = 0°$) for the experiment in Fig. 3. The parameter h is the water depth at the slope toe, for less idealised bathymetries the choice of the location of h is more challenging. The time series provide essential information such as the wave amplitudes a, heights H, celerity c and the wave type (Section 2.6). Fig. 4 indicates a cnoidal-like wave in proximity of the slide impact transforming into a Stokes-like wave further offshore, i.e. SLTs tend to become less non-linear with increasing distance from the slide impact. Fig. 4 illustrates the fast wave decay with increasing r; the maximum relative wave amplitude is $a_M/h = 0.57$ at $r/h = 3.0$ and $a_M/h = 0.040$ at $r/h = 35.0$, corresponding to a reduction by a factor of 14. Fig. 4 further illustrates the change of wave shape. This is mainly due to frequency dispersion, i.e. the SLT train consists of the superposition of wave components travelling at different speed (Sections 2.2 and 2.9). Sometimes dispersion results in an increased wave amplitude further offshore. Most of the aspects mentioned in this Section 2.1 are in more detail reviewed in follow-up sections.

2.2. Relevant parameters

The definition sketches in Fig. 2 show the relevant slide, water and tsunami parameters. SLTs depend on the

- Bulk slide volume ~~V_s~~ (or the slide grain volume ~~V_g~~ $= (1 - n/100)$~~V_s~~ (n = porosity))
- Bulk slide density ρ_s (or the grain density $\rho_g = \rho_s/(1 - n/100)$)
- Slide thickness s
- Slide length l_s
- Slide width b_s
- Slide impact velocity V_s
- Slide impact angle α
- Water depth (at the slope toe) h
- Water density ρ_w
- Gravitational acceleration g
- Slide model (block slide: sub-parameters: blockage ratio b_s/b (b = flume width), slide front angle ϕ, transition type; granular slide: sub-parameters: grain diameter d_g, grain size distribution, friction angles, porosity n, permeability coefficient k; viscoplastic slide: sub-parameters: rheology parameters, cohesion, etc.)
- Mass movement type (sliding, flowing, falling, toppling, spreading)
- Water body geometry (2D, 3D, intermediate geometries, etc.)
- Water body bathymetry
- Location (x in 2D, (r, γ) in 3D and intermediate geometries)

Once SLTs are generated, their propagation depends mainly on the geometry, bathymetry and frequency content. SLTs are modelled with Froude similarity in the laboratory (Hughes, 1993) implying that the gravity and inertial forces dominate over the kinematic viscosity of water ν_w (Reynolds number $R = g^{1/2}h^{3/2}/\nu_w$) and surface tension σ_w (Weber number $W = \rho_w g h^2/\sigma_w$). This requires a certain model size to

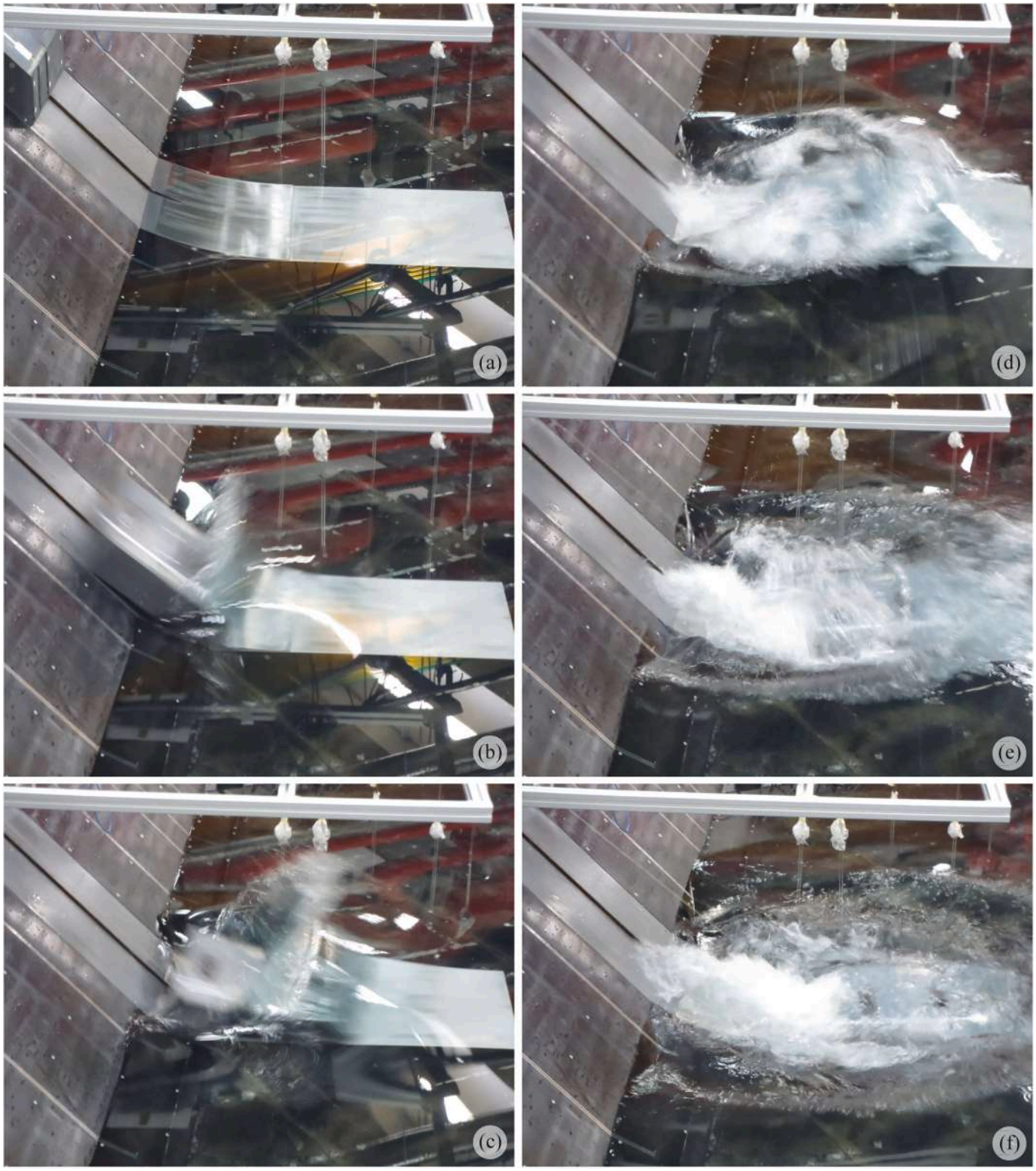

Fig. 3. Picture series of SLT generation in an idealised 3D laboratory experiment with a slide Froude number F = 1.52, a relative slide thickness $S = 0.50$ and a relative slide mass $M = 1.81$; the time interval from (b) onwards is 0.2 s (Heller et al., 2016).

avoid significant scale effects (Heller et al., 2008; Sauter et al., 2019; Kesseler et al., 2020). This is the case for R $\geq$ 300000 and W $\geq$ 5000 roughly corresponding to $h \geq 0.200$ m (Heller et al., 2008). These criteria were not always satisfied in SLT studies (Table 2) such that some wave parameters may be underestimated by some empirical equations due to scale effects. Both the slide centroid impact velocity (Fritz et al., 2004; Heller and Hager, 2010) and the slide front impact velocity (Huber and Hager, 1997; Mohammed and Fritz, 2012; Xue et al., 2019) are used to parameterise the granular slide kinematics. The slide thickness s can be defined as the maximum (Fritz et al., 2004) or an average measure of the slide thickness (Mulligan and Take, 2017) at impact.

Table 2
Generic subaerial and partially submerged landslide-tsunami studies with the geometry, slide model, main dimensions of the flume/basin, number of tests (6481 in total), investigated/predicted wave parameters and comments; for the meaning of the parameters and abbreviations see the notation and abbreviations sections at the end of this article.

Study	Geometry	Slide model	Dimensions flume/basin length [m] × b [m] × h [m]	Number of tests	Investigated/predicted wave parameters	Comments
Russell (1837)	2D	Block slide (RWG)	6.1 × 0.3 × 0.09 to 0.14	NA	c	Solitary wave investigation
Johnson and Bermel (1949)	3D	Block slide (disks)	19.5 × 37.2 × 0.24 to 0.31	56	$a_1(r)$, $L_1(r)$	Vertical falling discs to mimic the Bikini atomic bomb tests at 1:200
Law and Brebner (1968)	2D	Block slide (tray)	>9.0 × 0.61 × 0.23 to 0.43	47	H_M, $H(x)$, E_{pot}	Observed stable wave heights
Kamphuis and Bowering (1970)	2D	Block slide (tray)	45 × 1 × 0.23 to 0.46	≈50	H_M, T_1, $H(x)$, E_{pot}	Dimensional analysis, observed stable wave heights
Noda (1970); Wiegel et al. (1970)	2D	Block slide (RWG and piston)	32 × 0.3 × 0.15 to 0.61	≈120	a_M, $a(x)$	MM and laboratory experiments, wave type classification
Das and Wiegel (1972)	2D	Block slide (piston)	6.10 × 1.22 × 0.051 to 0.102; 8.23 × 0.15 × 0.076 to 0.305	≈80	a_M, a_1	Horizontally moving wall
Huber (1980); Huber and Hager (1997)	2D and 3D	Granular slide	30.4 × 0.5 × 0.12 to 0.36; 6 × 10 × 0.12 to 0.36	1000 (2D) + 150 (3D)	$H(x)$, $T(x)$, $L(x)$, $H(r, \gamma)$, E_{pot}	The experiments also involve snow avalanches and glacier calving data
Slingerland and Voight (1982)	3D, Mica Reservoir at 1:300 and Lake Koocanusa at 1:120	Bag-packed slide	1:300 (Mica Reservoir) and 1:120 (Lake Koocanusa)	20	a_M	Data from 2 case studies, relation between slide energy and a_M
Heinrich (1992)	2D	Block slide (triangular)	20 × 0.55 × 0.2 to 1.2	NA	Wave profiles	NM (Nasa-Vof2D) and laboratory experiments
Bukreev and Gusev (1996)	2D	Block slide (RWG)	4.3 × 0.2 × 0.04 to 0.08	NA	General observations	Mainly qualitative descriptions
Monaghan and Kos (2000)	2D	Block slide (RWG)	9 × 0.4 × 0.116 to 0.288	5	a_M	Experiments and NM (SPH)
Panizzo et al. (2002)	2D	Block slide (RWG)	4 × 0.11 × 0.06 to 0.23	135	Wave profiles	WT
Fritz et al. (2003a, 2003b); Fritz et al. (2004)	2D	Granular slide	11 × 0.5 × 0.3 to 0.675	137	a_M, L_1, E_{pot}	PIV, invention of pneumatic landslide generator, impact craters
Monaghan et al. (2003)	2D	Block slide	7 × 0.4 × 0.15 to 0.25	13	a_M	Experiments and NM (SPH)
Walder et al. (2003)	2D	Block slide	≈1 × 0.285 × 0.051 to 0.13	≈300	a_M, $\propto L_M$	Introduction of the characteristic time of submerged landslide motion
Zweifel (2004); Zweifel et al. (2006)	2D	Block and granular slides	11 × 0.5 × 0.15 to 0.60	86	a_M, $a(x)$	Comparison results of block and granular slides
Liu et al. (2005)	Narrow 3D	Block slide	104 × 3.7 × 2.44	72	$R_{e,M}$, $R_{e,t,M}$	Laboratory and NM (LES), planar hill slope, ≈70 underwater slide tests are not counted
Lynett and Liu (2005)	Narrow 3D	Block slide	$5l_s$ × $24b_s$ × NA	≈25	$R_{e,M}$	NM (depth-integrated, multilayer), ≈50 underwater slide tests are not counted
Panizzo et al. (2005b)	3D	Block slide	12 × 6 × 0.4 and 0.8	288	H_M, $H_M(r, \gamma)$, $T_M(r, \gamma)$, $a_1(r, \gamma)$, $H_1(r, \gamma)$, $T_1(r, \gamma)$	ANN, WT, mass impacted in the corner of a basin
Ataie-Ashtiani and Malek Mohammadi (2007)	Various	Natural slides	NA	11	a_M	Based on past cases in the field
De Carvalho and Do Carmo (2007)	2D	Slides consisting of blocks	12 × 1.0 × 0.30 to 0.55	20	a_M	Pressure measurements on the opposite shore

(*continued on next page*)

Table 2 (*continued*)

Study	Geometry	Slide model	Dimensions flume/basin length [m] × b [m] × h [m]	Number of tests	Investigated/predicted wave parameters	Comments
Heller (2007); Heller and Hager (2010); Heller and Hager (2011)	2D	Granular slides	11 × 0.5 × 0.15 to 0.60	211	a_M, H_M, T_M, $a(x)$, $H(x)$, $T(x)$, E_{kin}, E_{pot}	Established the impulse product parameter P, wave type classification
Ataie-Ashtiani and Nik-Khah (2008)	Narrow 3D	Block and granular slides	25 × 2.5 × 0.50 to 0.80	120	a_M, T_M, E_{pot}	Different block geometries
Heller et al. (2008)	2D	Granular slide	11 × 0.5 × 0.075 to 0.60	18	a_1, L_1, T_1, $H_1(x)$	Scale effects study
Di Risio et al. (2009a)	3D	Block slide	5.5 × 10.8 × 0.80	7	$R_{e,M}$, $R_{e,t,M}$, $R_{e,M}(r)$, $R_{e,t,M}(r)$	Planar hill slope, 4 underwater slide tests are not counted
Di Risio et al. (2009b); Romano et al. (2013); Bellotti and Romano (2017)	3D	Block slide	50 × 30 × 0.60 to 0.80	12	$R_{e,M}$, $R_{e,t,M}$, $R_{e,1}$, $R_{e,t,1}$, $R_{e,M}(r)$, $R_{e,t,M}(r)$, $R_{e,1}(r)$, $R_{e,t,1}(r)$	Conical hill slope, k-f spectral density
Sælevik et al. (2009)	2D	Block slide	25 × 0.51 × 0.60	3	General observations	PIV
Dong et al. (2010)	2D	Block slide	50 × 4.0 × 0.30	2	Wave profiles	WT, NM (FUNWAVE, Boussinesq equations), harbour resonance
Fuchs et al. (2010)	2D	Granular slide	11 × 0.5 × 0.20 to 0.45	3	General observations	Effect of the bathymetry
Heller et al. (2012)	2D, 3D and intermediate	Block slide	1.7 × 0.25 × 0.10; 2.1 × 2.0 × 0.10	8	$a(x)$, $H(x)$, $T(x)$, $a(r, \gamma)$, $H(r, \gamma)$, $T(r, \gamma)$,	Effect of the water body geometry, affected by significant scale effects
Mohammed and Fritz (2012)	3D	Granular slide	48.8 × 26.5 × 0.3 to 1.2	88	$a_1(r, \gamma)$, $a_{t,1}(r, \gamma)$, $L_1(r, \gamma)$, $T_1(r, \gamma)$, $a_2(r, \gamma)$, $L_2(r, \gamma)$, $T_2(r, \gamma)$, $R_{e,M}$, $R_{e,t,M}$, E_{pot}	WT
Heller and Spinneken (2013)	2D	Block slide	24.5 × 0.6 × 0.30 to 0.60	144	a_M, H_M, T of a_M, $a(x)$, $H(x)$ $T(x)$	Comparison with previous results from granular slides
Viroulet et al. (2013a)	2D	Block slide	18.0 × 0.65 × 0.38 to 0.43	NA	a_M	NM (SPHysics (SPH), Gerris (finite volume)) and laboratory experiments
Viroulet et al. (2013b); Viroulet et al. (2014)	2D	Granular slide	2.20 × 0.195 × 0.15	18	$a_{1,M}$, $a(x)$, E_{pot}	Experiments with low F (cliff collapse), effect of slide model, PIV
Huang et al. (2014)	Narrow 3D	Block and granular slides	24.5 × 5.5 × 0.45 to 0.85	74	$H_{1,M}$	Tests inspired by two past cases in the Three Gorges Reservoir
Evers and Hager (2015)	2D	Mesh-packed slide	11 × 0.5 × 0.20 to 0.40	42	a_M, H_M, $a(x)$, $H(x)$	Comparison results of mesh-packed slides with granular slides
Heller and Spinneken (2015); Heller et al. (2016)	2D, 3D and intermediate	Block slide	24.5 × 0.6 × 0.24 to 0.48; 20 × 12 × 0.24 to 0.48	48	$a_{1,M}$, $H_{1,M}$, $T_{1,M}$, $a_1(x)$, $H_1(x)$, $T_1(x)$, $R_{e,M}$, $R_{e,t,M}$, $R_{e,1}(r)$, E_{kin}, E_{pot}	Comparison SLTs in 2D and 3D, WT, PIV, pressure sensors in block front, NM (SPH) for intermediate geometries
Evers and Hager (2016); Evers et al. (2019a)	3D	Mesh-packed slide	8.0 × 4.5 × 0.20 to 0.40	74	a_1, $a_{t,1}$, a_2, $a_1(r, \gamma)$, $a_{t,1}(r, \gamma)$, $H_1(r, \gamma)$, $T_1(r, \gamma)$, $a_2(r, \gamma)$	Waves measured with videometric system
Lindstrøm (2016)	2D	Block and granular slides	7.3 × 0.25 × 0.20	5	Wave profiles	Effect of slide model
McFall and Fritz (2016); McFall and Fritz (2017)	3D	Granular slide	48.8 × 26.5 × 0.3 to 1.2	189	$a_1(r, \gamma)$, $a_{t,1}(r, \gamma)$, $H_1(r, \gamma)$, $T_1(r, \gamma)$, $L_1(r, \gamma)$, $R_{e,M}$, $R_{e,t,M}$, $R_{e,M}(r)$, $R_{e,t,M}(r)$, E_{pot}	Planar and divergent convex conical hill slopes
Wang et al. (2016)	Short 3D section of Yangtze River at 1:200	Slides consisting of blocks	20.0 × 8.0 × 0.50 to 1.00	49	H_M, H(reservoir axis)	OED
Zitti et al. (2016)	2D	Granular slide	2.5 × 0.11 × 0.11 to 0.18	42	a_M, H_M, E_{pot}	Snow avalanches
Bregoli et al. (2017); Bregoli et al. (2020a, 2020b)	3D	Granular slide	4.1 × 2.45 × 0.20 to 0.25	41	a_M, $a_1(r, \gamma = 0°)$, E_{pot}	Waves measured with laser grid

(*continued on next page*)

Table 2 (*continued*)

Study	Geometry	Slide model	Dimensions flume/basin length [m] × b [m] × h [m]	Number of tests	Investigated/predicted wave parameters	Comments
Huang et al. (2017)	Very narrow 3D	Block slide	5.0 × 1.5 × 0.20 to 0.40	25	a_1, L_1	The slides did not fully submerge, OED
Mulligan and Take (2017); Miller et al. (2017)	2D	Granular slide	33.0 × 2.09 × 0.05 to 0.50	8	a_M, $a(x)$	PIV for the granular slide
Wang et al. (2017); Wang et al. (2019b)	Short 3D section of the Yangtze River	Block slide	8 × 20 × 0.50 to 1.00	49 + 49	a_1, a_M, a_2	Impact perpendicular to channel axis, dimensions reduced due to bathymetry, OED
Meng (2018); Meng and Ancey (2019); Meng et al. (2020)	2D	Granular and viscoplastic slides	1.5 × 0.12 × 0.20; 2.5 × 0.12 × 0.20	553	a_M, H_M, L_M	Effect of slide model, ANN
Tang et al. (2018)	2D	Block and granular slides and mixtures	20.5 × 0.4 × 0.3	73	a_M, $a(x)$	Effects of slide model, WT
Wang et al. (2018)	2D	Block slide	9 × 0.5 × 0.25 to 0.45	25	H_M, $H(x)$	OED
Bullard et al. (2019a, 2019b)	2D	Water slide	33.8 × 2.1 × 0.15 to 0.65	41	a_M	Acoustic Doppler current profiler, wave profile asymmetry
Heller et al. (2019); Heller et al. (2021)	3D	Block slide	50 × 50 × 0.75 to 1.00	35	a_M, H_M, $a(r, \gamma)$, $H(r, \gamma)$, E_{pot}	Iceberg calving, effect of mass movement type, 31 buoyancy-dominated and capsizing tests are not counted
Ruffini et al. (2019)	2D, 3D and intermediate	Predefined waves	28.3 × 0.6 × 0.30 to 0.60 up to 28.3 × 64.0 × 0.30 to 0.60	24	$a(x)$, $H(x)$, $a(r, \gamma)$, $H(r, \gamma)$	NM (NH-NLSWEs), effects of diverging water body geometries in the far field
Tessema et al. (2019)	Short 3D	Block slides	1.7 × 4.5 × 0.288 to 0.296	66	Dam overtopping volume	Impact perpendicular to channel axis
Xue et al. (2019)	2D	Granular slide	10 × 0.6 × 0.20 to 0.50	49	a_M, H_M, T_1, $H(x)$, $T(x)$, $\eta(x)$	Semi-theoretical equation for the free surface elevation for Stokes-like waves, OED
Yavari-Ramshe and Ataie-Ashtiani (2019)	2D section of the Maku dam reservoir at 1:1	Granular slide	220 × NA × 50	78	a_M, $a_{t,M}$, H_M, E_{kin}, E_{pot}	Variation of the geotechnical and rheological properties, 39 underwater slide tests are not counted
Zhao and Yao (2019)	Idealised 3D section of Midui ice lake	Granular slide	3.76 × 1.51 × 0.10 to 0.30	18	H_M	Waves affected by reflection, similar as in the Midui ice lake
Bougouin et al. (2020)	2D	(Fluidised) granular slide, water slide	7 × 0.2 × 0.13 to 0.39	≈20	a_1, L_1	Tests with/without air entrainment through the hill slope
Deng et al. (2020)	Short 3D	Block slide	1.5 × 60 × 0.4 to 0.7	31	H_M, $H_M(r, \gamma)$	Experiments and NM (FLOW-3D, RANS equations)
De Lange et al. (2020)	3D	Debris flow	1.85 × 0.90 × 0.0 to 0.33	60	$a_{1,M}$, L_1	Basin floor inclined at 10°
Huang et al. (2020)	2D	Granular column	16 × 0.3 × 0.0 to 0.5	52	a_M	Granular column collapse in water, PIV, wave type classification
Mu et al. (2020)	Short 3D section of Yangtze River at 1:70	Slides consisting of blocks	48 × 28 × 0.74 to 1.16	81	a_M, H_M, $a_M(r, \gamma)$	Effects on moored ships
Takabatake et al. (2020)	2D	Granular slide	14.5 × 0.4 × 0.15 to 0.65	164	a_1, $a_{t,1}$, T_1, L_1, a_2, T_2, L_2	Subaerial, partially submerged and

(*continued on next page*)

Table 2 (*continued*)

Study	Geometry	Slide model	Dimensions flume/basin length [m] × b [m] × h [m]	Number of tests	Investigated/predicted wave parameters	Comments
						underwater slide tests, 97 underwater slide tests are not counted
Zhang et al. (2020)	3D, lateral diverging and converging	Granular slide	6600 × 3000 × 100; 6600 × 500 × 100	14	$a(r, \gamma)$, $a_t(r, \gamma)$, $H(r, \gamma)$	NM (Tsunami Squares) at full scale, effect of the water body geometry
Franco et al. (2021)	Short 3D	High density water slide	250 to 3000 × 500 to 12000 × 10 to 100	69	$a(r, \gamma)$	Investigation of idealised lake shapes, NM (FLOW-3D, RANS equations)
Rauter et al. (2021)	2D	Water slide	33.8 × 2.1 × 0.15 to 0.65; 10.0 × 2.1 × 0.15 to 0.90	144	a_M	NM (OpenFOAM, RANS equations)
Robbe-Saule et al. (2021)	2D	Granular column	2.0 × 0.15 × 0.02 to 0.12	≈48	a_M, L_M	Granular column collapse
Ruffini et al. (2021)	2D and 3D	Predefined waves	Up to 45.2 × 0.6 × 0.30 to 0.60; 45.2 × 77.0 × 0.30 to 0.60	184	$a(x)$, $H(x)$	NM (NH-NLSWEs), ANN, effect of the bathymetry
Sarlin et al. (2021)	2D	Granular column	2.0 × 0.15 × 0.02 to 0.25	≈80	a_M, L_M	Granular column collapse, wave type classification
Feng et al. (2022)	2D	Block slide	20 × 0.0 × 0.30	35	H_M	ML, NM (Immersed Boundary Method and Lattice Boltzmann method)
Han et al. (2022)	3D	Slides consisting of blocks	48 × 8.0 × 0.40 to 1.16	135	Wave profiles	Wave type classification
Huang and Chan (2022)	2D	Block slide	20 × 0.55 × 0.40	9	a_1, a_2, a_M, T, E_{pot}	NM (OpenFOAM, RANS equations)
Hu et al. (2022)	2D	Granular slide	NA × 0.4 × 0.10 to 0.60	19	a_M	Wave type classification
Lee and Huang (2022)	2D	Granular slide	2.3 × 0.15 × 0.14	4	H_1	Effect of grain diameter, laboratory experiments and NM (multi-phase flow model)
Liu et al. (2023a, 2023b)	Short 3D	Block slide	4.45 × 23.0 × 0.20 to 0.34	115	$a(r, \gamma)$, $H(r, \gamma)$, $R_{e,M}$, $R_{e,1}(r)$	WT
Sabeti and Heidarzadeh (2022)	2D	Block and granular slides	4.0 × 0.26 × 0.150 to 0.246	52	a_M	Comparison results of block slides with granular slides, NM (FLOW-3D-Hydro)
Li et al. (2023)	3D and very narrow 3D	Slides consisting of 1 to 16 blocks	45.0 × 80.0 × 4.0 to 7.0; 6.00 × 0.35 × 0.30	49 + 192	a_M	Laboratory experiments and NM (RANS equations)
Wang et al. (2023)	2D	Block slide	NA × 0.66 × 0.86 to 1.26	18	a_1, E_{pot}	V-shaped geometry, OED

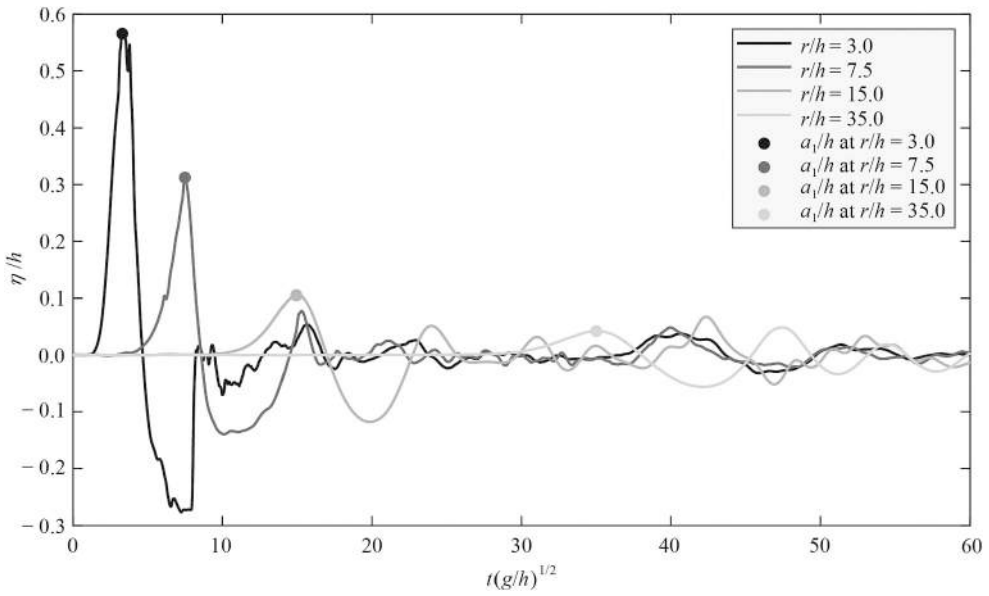

Fig. 4. Relative water surface elevation η/h versus relative time $t(g/h)^{1/2}$ along the slide axis $\gamma = 0°$ for r/h = 3.0, 7.5, 15.0 and 35.0 for the experiment shown in Fig. 3.

Using dimensional analysis (Buckingham, 1914) with the reference parameters h, ρ_w and g, the first 10 parameters and the last one above are transformed into the dimensionless parameters

- Relative slide volume $V = \forbidden{V}_s/h^3$
- Relative slide density $D = \rho_s/\rho_w$
- Relative slide thickness $S = s/h$
- Relative slide length $L_s = l_s/h$
- Relative slide width $B = b_s/h$
- Slide Froude number $\mathrm{F} = V_s/(gh)^{1/2}$
- Slide impact angle α
- Relative distance x/h or radial distance r/h and wave propagation angle γ

There is some flexibility in the literature about the use of these dimensionless parameters depending on the specific experimental conditions, e.g. $\forbidden{V}_s$, s, b_s and l_s are dependent ($\forbidden{V}_s \propto sb_sl_s$) such that one of them should be excluded, particularly for block studies. Some authors merged some of these dimensionless parameters, e.g. Zweifel et al. (2006) introduced the relative slide mass $M = VD/B = m_s/(\rho_w b_s h^2)$, where $m_s = \forbidden{V}_s\rho_s$ is the slide mass. No established dimensionless parameters to fully quantify the slide model (Section 2.4), mass movement type, water body geometry (Section 2.7) and bathymetry (Section 2.8) are currently available, but some promising options are reviewed in later sections.

Variations of the dimensionless parameters allow for the derivation of (semi-)empirical equations for the unknown wave parameters. Most studied are the maximum wave amplitude a_M, height H_M and period T_M (or wavelength L_M) in the slide impact zone and their evolutions with distance $a(x)$, $H(x)$ and $T(x)$ (or $L(x)$) in 2D or $a(r, \gamma)$, $H(r, \gamma)$ and $T(r, \gamma)$ (or $L(r, \gamma)$) in 3D (Fig. 2), such that the effects of SLTs at any point in a water body can be predicted. For example, Heller and Hager (2010) derived empirical equations for 2D granular slides to predict these 6 parameters under systematic variation of F, S, D, V (or M), α and the relative grain diameter d_g/h (with a negligible effect in the investigated range, Section 2.4). These results were expressed in function of the impulse product parameter $\mathrm{P} = \mathrm{F}S^{1/2}M^{1/4}\{\cos[(6/7)\alpha]\}^{1/2}$. The proposed semi-empirical equations for $a_{2D,M}$ and $a(x)$ are

$$a_{2D,M}/h = (4/9)\mathrm{P}^{4/5} \tag{1}$$

$$a(x)/h = (3/5)\left[\mathrm{P}(x/h)^{-1/3}\right]^{4/5} \tag{2}$$

Corresponding examples of empirical equations for 3D based on block slides under variation of F, S and V (or M) were provided by Heller and Spinneken (2015) for the maximum primary (subscript 1) wave as

$$a_{3D,1,M}/h = 0.50\left(\mathrm{F}S^{1.10}M\right)^{0.85} \tag{3}$$

$$a_{1,M}(r,\gamma)/h = 1.75\mathrm{F}^{0.80}S^{1.25}M^{0.67}(r/h)^{-1.0}cos^{2\{1+exp[-0.2(r/h)]\}}(2\gamma/3) \tag{4}$$

Most studies conclude that F and S are particularly important parameters for SLT generation.

2.3. Generic SLT studies

Nearly all relevant parameters in Section 2.2 have been investigated, but never within a single study (Section 3.2). Most studies varied 4 - 5 parameters or even less. Table 2 includes past subaerial and partially submerged generic landslide-tsunami studies with information on the water body geometry, slide model, main dimensions of the used flume/basin, number of tests, investigated/predicted wave parameters and comments. This includes 76 generic SLT studies (98 publications) comprising altogether 6481 individual experiments. 10 important milestone studies in Table 2, applying a new method or proposing something for SLTs for the first time, are in the authors personal view:

- Russell's (1837) Wave Generator (RWG) may be regarded as the initiation of SLT research
- Noda (1970) classified and systematically described the wave types of SLTs as oscillatory, non-linear transient, solitary and bore waves
- Huber and Hager (1997) reanalysed the 1150 systematic 2D and 3D granular slide tests of Huber (1980) to derive empirical equations for both 2D and 3D conditions which remained the most important equations for SLT prediction for over a decade
- Panizzo et al. (2002) analysed SLTs for the first time with a frequency domain analysis method (the wavelet transform WT)
- Fritz et al. (2004) developed the pneumatic landslide generator allowing to independently vary the granular slide parameters (e.g. V_s and α, or V_s and s) to meet this fundamental requirement of

dimensional analysis; they further used Particle Image Velocimetry (PIV) for the first time providing insight into the kinematics of SLTs
- Lynett and Liu (2005) investigated edge waves for the first time for SLTs
- Panizzo et al. (2005b) used Artificial Neural Network (ANN) for the first time for the analysis of SLTs
- Heller and Hager (2010) introduced the impulse product parameter P to correlate all relevant SLT parameters in practice in 2D
- Mohammed and Fritz (2012) used similar techniques as Fritz et al. (2004) to conduct granular slide tests in a large wave basin (3D)
- Ruffini et al. (2019) derived semi-empirical equations linking SLTs in 3D and intermediate geometries to 2D

Most studies in Table 2 concentrated on the maximum SLT features a_M and H_M. Only a small number of studies predicted the wave parameter evolutions (e.g. $a(x)$, $H(x)$, $a(r, \gamma)$, $H(r, \gamma)$), although they are key to compute the wave runup on opposite shores or structures. Investigations of the wave period T are also mentioned in Table 2. Excluded from Table 2 is a systematic mention of the wave celerity c because it is well established (Kamphuis and Bowering, 1970; Huber, 1980; Fritz et al., 2004; Heller and Spinneken, 2013; amongst others) that c_1 can be approximated using solitary wave speed, e.g. Laitone (1960) derived the speed for a 1st order stable solitary wave on a mild slope as

$$c = [1 + a/(2h)](gh)^{1/2} \quad (5)$$

More generalised formulations than Eq. (5) are available if considering e.g. wave instability (Tanaka, 1986) or higher order terms. Eq. (5) reduces for small waves $a \to 0$ to the linear shallow-water wave celerity

$$c = (gh)^{1/2} \quad (6)$$

Table 2 illustrates the increased SLT research effort in the 1970ties motivated by the 1958 Lituya Bay case and two further cases in Italy in 1959 and 1963 (Table 1). Another more significant research boom was initiated in 2000, which is still ongoing (over 75% of the studies in Table 2 have been conducted after 2005). Approximately 50% of the studies in Table 2 are from authors based in Europe with particularly productive groups based in mountainous countries such as Italy and Switzerland. Contributions from colleagues from China over-proportionally increased in the last decade, motivated by 3 cases in the Three Gorges Reservoir (Table 1). Last but not least, numerical studies, e.g. based on SPH (e.g. Viroulet et al., 2013a; Heller et al., 2016) or the Reynold-averaged Navier-Stokes (RANS) equations (e.g. Deng et al., 2020; Rauter et al., 2021; Li et al., 2023), are more and more used, given that the computer power significantly increased over the last decade. This trend is likely to continue (Section 4.3).

2.4. Effects of mass movement type and slide model

2.4.1. Mass movement type

The mass movements can be classified according to Cruden and Varnes (1996) into five types (Fig. 5): (a) sliding with rotation along a curved concave slide plane or translation on a plane, (b) flowing with a similar behaviour as a viscous fluid, (c) falling with free-falls typically observed for $\alpha > 76°$, (d) toppling with movement relative to a rotation point/axis located below its centre of gravity and (e) spreading observed for $0.3° \leq \alpha \leq 5°$.

A limited amount of research has been conducted into the effect of the mass movement type on SLTs. The RWG (Russell, 1837; Noda, 1970; Bukreev and Gusev, 1996; Monaghan and Kos, 2000; Panizzo et al., 2002) corresponds to an idealised fall case. Tsunamis generated by idealised fall and toppling cases (Fig. 5c,d) have been compared by Heller et al. (2019, 2021) in the context of iceberg calving in 3D. The overturning (toppling) icebergs tend to generate larger a_M and H_M than icebergs vertically falling into water. However, this trend reversed in the wave propagation zone ($H(r, \gamma)$ and $a(r, \gamma)$) where the waves were larger for the fall than the overturning cases (Heller et al., 2021). Granular column collapse experiments are related to the fall case and have recently been investigated for both columns initially located out of (Robbe-Saule et al., 2021; Sarlin et al., 2021) and in the water body (Huang et al., 2020). As expected, the observed wave types in these

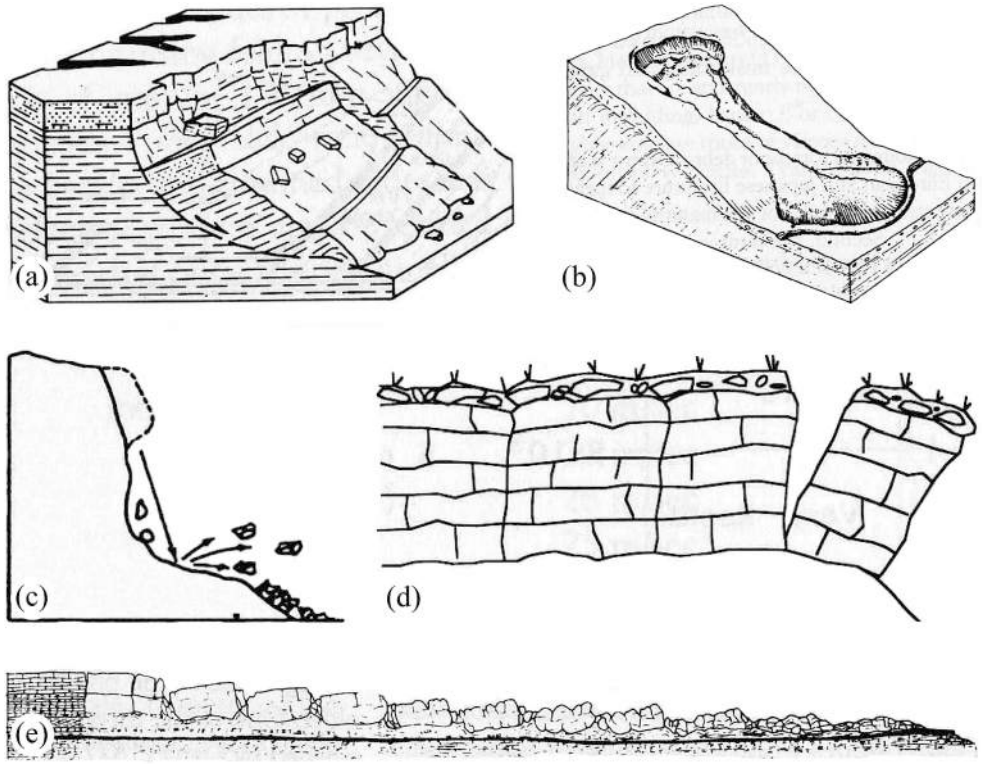

Fig. 5. Mass movement types: (a) sliding, (b) flowing, (c) falling, (d) toppling and (e) spreading (after Cruden and Varnes, 1996).

column collapse studies are very similar as for slides (Section 2.6). However, there are also some stark differences for some relevant parameters, e.g. the observed effect of the grain density in the range 30 - 6780 kg/m^3 on a_M is small in the experiments of Robbe-Saule et al. (2021). In contrast, the slide density has a stronger effect for sliding cases (Heller and Hager, 2010; Zitti et al., 2016).

A range of slide rheologies have also been investigated. Flowing (Fig. 5b) is represented by viscoplastic slides (Meng and Ancey, 2019; Meng et al., 2020), debris flows (De Lange et al., 2020), pyroclastic flows (Bougouin et al., 2020; Lipiejko et al., 2022) and slides modelled with water (Bullard et al., 2019a, 2019b). Viscoplastic slides generate on average approximately 30% (Meng and Ancey, 2019) and water slides between 0 - 200% (Fig. 13 in Bullard et al., 2019a; Bougouin et al., 2020) larger a_M than corresponding granular slides.

Landslide-tsunamis have also been modelled with a piston-type wave generation mechanism by Noda (1970) and Das and Wiegel (1972) being related to the spreading mass movement type (Fig. 5e). However, the wall in front of the piston was impermeable and taller than the generated wave such that these studies may predict significantly larger relative wave heights than observed in the field.

2.4.2. Slide model

The slide model, i.e. the composition of the slide, is somehow related to the mass movement type, e.g. granular slides are strongly linked to sliding (Fig. 5a) and debris flows to flowing (Fig. 5b). Most studies model slides with a block or granular material, rarer used are mesh-packed granular materials (Evers et al., 2019a), several blocks (De Carvalho and Do Carmo, 2007; Wang et al., 2016; Mu et al., 2020; Li et al., 2023), mixtures of a block and granular material (Tang et al., 2018), debris flows (De Lange et al., 2020), fluidised granular material (Bougouin et al., 2020), viscoplastic materials (Meng and Ancey, 2019; Meng et al., 2020) and water as an upper high mobility limit (Bullard et al., 2019a, 2019b) (Table 2).

Whilst block slides allow for a simpler experimental handling, they can be more delicate in terms of wave generation than granular slides. Three block model parameters affect wave generation: (i) the blockage ratio (b_s/b in 2D), (ii) the slide front angle ϕ (Fig. 2a) and (iii) the transition type at the slope toe (e.g. no transition (Fig. 2a) with abrupt block stop as an extreme case, circular transition with smooth block runout) (Heller and Spinneken, 2013). Granular slides behave less complex as they fill the entire flume width ($b_s/b = 1.0$), $\phi \approx 90°$ during impact and their deformability allows them to runout relatively smoothly, even for abrupt transitions at the slope toe. A direct comparison between block (with $b_s/b = 0.98$, $\phi = 90°$ and a circular transition) and granular slides shows that blocks generate on average 1.3 to 1.9 times larger a_M, H_M, $a(x)$ and $H(x)$ than granular slides under otherwise identical conditions (Fig. 12 of Heller and Spinneken, 2013; Evers et al., 2019a). This finding is supported by Ataie-Ashtiani and Nik-Khah (2008), Zweifel (2004), Tang et al. (2018) and Sabeti and Heidarzadeh (2022), who also found block slides to generate larger waves. However, block slides may sometimes generate significantly smaller waves than granular slides if the block abruptly stops at the channel/basin bottom (Heller and Spinneken, 2013).

Cohesion is a major difference between block (infinite cohesion) and granular slides (low to no cohesion). Meng and Ancey (2019) investigated viscoplastic slides made of polymeric gel of different cohesions and compared the wave amplitude to the one from granular slides. Their viscoplastic slides generated approximately 50% larger H_M and 30% larger a_M, but approximately 40% shorter wavelengths than granular slides. Related numerical work has also been conducted by Yavari-Ramshe and Ataie-Ashtiani (2019) by investigating the effects of geotechnical and Coulomb rheological parameters (n, internal friction angle, basal friction angle, ρ_s, constitutive parameters). As expected, H_M increases with increasing ρ_s, and decreases with both increasing n and the basal friction angle.

Based on a block and four different granular materials, Lindstrøm (2016) used the permeability coefficient k of the slide, given by the Kozeny-Carman equation (Carrier, 2003), to explain the change in SLT magnitude in function of the slide model. If the slide velocity $V_s < k$, then water penetrates into the slide instantaneously when the slide impacts the water body, resulting in a reduced SLT compared to the one generated by a block. On the other hand, if $V_s > k$, the slide will not be instantaneously saturated by water during wave generation and the generated SLT agrees better with waves generated by block slides. This concept is in line with the previous finding that the difference between SLTs generated by blocks and granular slides decreases with increasing F (Zweifel, 2004). This also explains that Heller and Hager (2010) and Lipiejko et al. (2022) found a negligible effect of the grain size distribution on SLTs in the range $0.003 \leq d_g/h \leq 0.04$ and $d_g/h \leq 0.03$, respectively. For larger grain diameters, on the other hand, Huang et al. (2014) ($0.008 \leq d_g/h \leq 0.154$) and Hu et al. (2022) ($0.003 \leq d_g/h \leq 0.100$) found that this effect is not negligible. As expected, these limits change for granular slides impacting at low F; for $F \leq 0.8$, Viroulet et al. (2014) found a small effect on a_M for $0.027 \leq d_g/h \leq 0.067$. The limits are also different for granular column collapses for which Robbe-Saule et al. (2021) found a negligible effect on a_M in the range $0.02 \leq d_g/h \leq 0.16$. The block model parameters, cohesion and k are promising concepts to fully understand the effect of the slide model.

2.5. Slide to wave energy transfer

The amount of energy transferred from the slide to the waves is relevant allowing, once the slide release location and mass are known, to compute how much energy is available for SLT generation. Table 3 includes studies from Table 2, complemented with further numerical studies, which addressed this energy transfer. In most studies the slide energy E_s was defined as the kinetic slide energy at impact $E_s = m_s V_s^2/2$. Alternatively, Ataie-Ashtiani and Nik-Khah (2008) and Wang et al. (2023) used $E_s = \rho_s V_s^2 A$, with the cross-sectional area of the slide A, and Viroulet et al. (2014) and Heller et al. (2019) used the potential slide energy difference between initial and final positions as a reference for the wave energy. Apart from Heller (2007), Heller et al. (2016), Clous and Abadie (2019), Yavari-Ramshe and Ataie-Ashtiani (2019) and Feng et al. (2022), the kinetic wave energy E_{kin} was not directly measured but assumed to be identical to the potential wave energy E_{pot}, although this equipartition concept from linear wave theory is not always a good assumption for SLTs (Heller, 2007; Mohammed and Fritz, 2012; Heller et al., 2016). In most studies, E_{pot} was extracted from the wave train passing a specific location at a certain wave speed whilst Heller (2007) calculated E_{pot} over an area based on PIV frames and E_{pot} can also be obtained over an area in numerical simulations (e.g. Yavari-Ramshe and Ataie-Ashtiani, 2019; Feng et al., 2022).

Despite this range of methods and assumptions to extract E_{pot} and E_{kin} and a wide range of transferred energies between 1 and 90% over all studies in Table 3, some trends can be revealed. 2D studies tend to result in larger energy transfers (1 - 90% overall) than 3D studies (1 - 56.9%), given that in 3D water escapes laterally and flows around the landslide decreasing the efficiency of wave generation (Mohammed and Fritz, 2012). Further, 3D block slides (2.4 - 56.9%) tend to be more efficient than 3D granular slides (1 - 24%), which is expected due to internal dissipations in granular slides (Viroulet et al., 2014; Kesseler et al., 2020). On the other hand, blocks may stop abruptly at transitions at the slope toe such that a large part of the block slide energy is transferred to the channel/basin bottom (Heller and Spinneken, 2013). This explains why 2D block slides are not always more efficient than 2D granular slides (Table 3).

A direct link between the slide energy and the wave energy would be useful, however, the large scatter from 1 to 90% in Table 3 illustrates that this is rather challenging. It is also a major challenge to relate the relevant wave parameters (a_M, $H_M(x)$, etc.) to this energy transfer given that sometimes not the full slide mass is involved in wave generation (Viroulet et al., 2014; Miller et al., 2017; Meng, 2018) and SLTs can

Table 3
SLT studies investigating the slide to wave energy transfer with information about the geometry, slide model, number of tests (2368 in total), slide to wave energy transfer and comments including the main assumptions; values with superscript 1 include the primary wave and with 1,c the wave crest of the primary wave only.

Study	Geometry	Slide model	Number of tests	$(E_{pot} + E_{kin})/E_s \times 100$ [%]	Comments
Law and Brebner (1968)	2D	Block slide (tray)	47	2 - 28	$E_s = m_s V_s^2/2$
Kamphuis and Bowering (1970)	2D	Block slide	≈50	10 - 50	$E_s = m_s V_s^2/2$, assumption $E_{kin} = E_{pot}$
Huber (1980)	2D	Granular slide	1000	1 - 40	$E_s = m_s V_s^2/2$, assumption $E_{kin} = E_{pot}$
Ward and Asphaug (2003)	3D	Block slide	1	9.4	$E_s = m_s V_s^2/2$, assumption $c = 0$ ($E_{kin} = 0$) at the impact location, hypothetical asteroid impact
Fritz et al. (2004)	2D	Granular slide	137	4 - 50; 2 - 30[1, c]	$E_s = m_s V_s^2/2$, assumption $E_{kin} = E_{pot}$
Heller (2007)	2D	Granular slide	211	11.3 - 85.7	$E_s = m_s V_s^2/2$, E_{kin} measured for the wave train with PIV when the primary wave front reached $8h$ for $0 \leq x \leq 8h$, E_{pot} extracted from the same area
Ataie-Ashtiani and Nik-Khah (2008)	Narrow 3D	Block and granular slides	120	4 - 5	$E_s' = \rho_s V_s^2 A$, assumption $E_{kin} = E_{pot}$
Mohammed and Fritz (2012)	3D	Granular slide	88	1 - 15, 0.5 - 4[1,c]	$E_s = m_s V_s^2/2$, assumption $E_{kin} = E_{pot}$, E_{pot} measured with wave probes at ($10h$, γ), the first 3 waves of the wave train were considered
Viroulet et al. (2014)	2D	Granular slide	18	< 15	E_s = potential slide energy difference between initial and final positions, low F (cliff collapse), assumption $E_{kin} = E_{pot}$
Heller et al. (2016)	2D	Block slide	2	18[1], 47[1]	$E_s = m_s V_s^2/2$, E_{kin} and E_{pot} measured with wave probes and PIV at $x/h = 5.0h$, $7.5h$, $10.0h$ and $15.0h$
McFall and Fritz (2016)	3D	Granular slide	159	1 - 24, 0.5 - 11[1,c]	$E_s = m_s V_s^2/2$, assumption $E_{kin} = E_{pot}$, the first 3 waves in the wave train were considered
Zitti et al. (2016)	2D	Granular slide	42	2.6 - 21	$E_s = m_s V_s^2/2$, assumption $E_{kin} = E_{pot}$, E_{pot} extracted from camera frames
Bregoli et al. (2017)	3D	Granular slide	41	4.7 - 8.1[1,c]	$E_s = m_s V_s^2/2$, assumption $c = 0$ ($E_{kin} = 0$) at the impact location
Meng and Ancey (2019)	2D	Granular and viscoplastic slides	157	9 - 30	$E_s = m_s V_s^2/2$ with the effective slide mass for m_s, assumption $E_{kin} = E_{pot}$
Clous and Abadie (2019)	2D	Newtonian fluid	1	30	Slide energy consisting of kinetic and potential energy relative to flume bottom, both E_{kin} and E_{pot} were considered
Heller et al. (2019)	3D	Block slide	35	2.4 - 56.9	Only gravity-dominated tests are considered, E_s = potential slide energy difference between initial and final positions, assumption $E_{kin} = E_{pot}$, E_{pot} measured with wave probes at ($2h$, γ)
Yavari-Ramshe and Ataie-Ashtiani (2019)	2D	Granular slide	39	5 - 15	$E_s = m_s V_s^2/2$ + potential energy relative to basin bottom, wave energy extracted over the entire 2D domain
Bregoli et al. (2020a)	3D	Granular slide	23	6	$E_s = m_s V_s^2/2$ + potential energy relative to basin bottom, assumption $E_{kin} = E_{pot}$, semi-theoretical
Feng et al. (2022)	2D	Block slide	35	40.3 - 60.2	E_s = potential slide energy difference between initial and final positions, E_{kin} and E_{pot} of the entire water body at the moment when the slide stops
Han et al. (2022)	3D	Slides consisting of blocks	135	1 - 18, 0.5 - 7[1,c]	$E_s = m_s V_s^2/2$, assumption $E_{kin} = E_{pot}$, the first 3 waves in the wave train were considered
Huang and Chan (2022)	2D	Block slide	9	22 - 90	$E_s = m_s V_s^2/2$, assumption $E_{kin} = E_{pot}$
Wang et al. (2023)	2D	Block slide	18	8 - 44	$E_s' = \rho_s V_s^2 A$, assumption $E_{kin} = E_{pot}$

consist of one or several waves which can be intermediate- to shallow-water waves, i.e. the wave energy is not uniformly distributed over the wave train and water column.

2.6. Wave types

The wave types of SLTs are relevant to classify SLTs and to link them to Stokes (Fenton, 1985), cnoidal (Fenton, 1999) and solitary wave theories (Boussinesq, 1872) as well as dispersive combinations. Further, some SLT features strongly depend on the wave type including their decay, frequency dispersion and their celerity (Ruffini et al., 2019). SLTs are typically non-linear intermediate- to shallow-water waves (Fritz et al., 2004; Heller and Hager, 2011). Their profiles are often linked to non-linear wave theories (Stokes, cnoidal, solitary) (Heller et al., 2016; Xue et al., 2019), typically affected by wave dispersion. SLT generation often involves a violent slide-water momentum transfer (Fig. 3). If $F > 1$, then local flow separation, backward collapsing impact craters or outward collapsing impact craters are observed (Fritz et al., 2003a, 2003b). Once wave generation is completed, some distance from the slide impact, SLTs become stable in the so-called wave propagation zone. The location of the start of the wave propagation zone may be estimated with the streamwise distance x_M of Heller and Hager (2010), the impact radius r_0 of Evers et al. (2019a) or the length of the wave generation zone Δx_g of Xue et al. (2019). The wave type is often not stable, i.e. it adapts and changes with propagation distance due to lateral energy spread and dispersion. The most energetic wave types (bore- and solitary-like waves) close to the slide impact transform further offshore to less energetic and more linear waves such as cnoidal- or Stokes-like waves, i.e. they may approach Airy's asymptotic solution sufficiently far away from the source (Løvholt et al., 2008).

Wave type classifications are aimed at predicting the wave type in function of the dimensionless parameters (Section 2.2). Classifications apply to a specific slide type, water body geometry and location (x or r, γ), i.e. the wave type observed for specific dimensionless parameters may differ for granular and block slides and the most energetic wave types (solitary- and bore-like waves) in 2D are only observed in the slide impact zone on the slide axis in 3D, if at all (Mohammed and Fritz, 2012; Heller and Spinneken, 2015; Han et al., 2022). Wave type classifications for 2D (Noda, 1970; Wiegel et al., 1970; Huber, 1980; Fritz et al., 2004; Zweifel et al., 2006; Heller and Hager, 2011; Heller and Spinneken, 2015; Bullard et al., 2019b; Xue et al., 2019; Huang et al., 2020; Sarlin et al., 2021) and 3D (Panizzo et al., 2005b; Mohammed and Fritz, 2012; Heller and Spinneken, 2015; Han et al., 2022) rely on five approaches: (i) optical wave profile inspection (Noda, 1970; Wiegel et al., 1970; Huber, 1980; Fritz et al., 2004; Heller and Hager, 2011; Heller and Spinneken, 2015; Xue et al., 2019; Huang et al., 2020; Han et al., 2022), (ii) non-linearity a/H (Zweifel et al., 2006), (iii) Ursell parameter $U = (H/h)(L/h)^2 = HL^2/h^3$ (Huber, 1980; Panizzo et al., 2005b), (iv) Hilbert transform (Bullard et al., 2019b) and (v) frequency domain analysis methods (Panizzo et al., 2002, 2005b; Heller and Spinneken, 2015; Brühl and Becker, 2018).

A linear wave based on method (ii) requires $a/H = 0.5$ and a solitary wave $a/H = 1$. The Ursell parameter $U \to 0$ is a more appropriate criterion to identify linear waves than simply $a/H = 0.5$ as linear waves not only show identical crest and trough amplitudes, but also small ratios of

H/h and H/L (Ursell, 1953). The value of U further indicates Stokes waves U < 10, Stokes and cnoidal waves (10 ≤ U ≤ 26), cnoidal waves (U > 26) and solitary waves (U ≈ 1) (Dingemans, 1997). The Hilbert transform was used by Bullard et al. (2019b) to classify SLTs with the wave asymmetry. Frequency domain analysis methods predict the wave type indirectly by comparing the speed, at which SLT energy components propagate, with theoretical wave speed in the case of the wavelet transform (WT) (Panizzo et al., 2002, 2005b; Heller and Spinneken, 2015; Tang et al., 2018) and directly by evaluating the modulus within the Korteweg-de Vries equations (Brühl and Becker, 2018) (Section 4.2).

Fig. 6 shows the generation and propagation as well as the corresponding wave profiles of the full range of wave types observed in 2D namely Stokes-, cnoidal-, solitary- and bore-like waves (Heller and Hager, 2011; Xue et al., 2019). More refined terms have sometimes been applied to describe SLTs such as weakly non-linear oscillatory waves, oscillatory waves, non-linear transient waves or (dissipative) transient bores (Noda, 1970; Wiegel et al., 1970; Huber, 1980; Fritz et al., 2004; Panizzo et al., 2005b; Zweifel et al., 2006; Heller and Hager, 2011; Bullard et al., 2019b; Han et al., 2022). Recent research (Brühl and Becker, 2018) revealed that SLTs are a superposition of linear, Stokes, cnoidal and solitary waves and their non-linear interactions (Section 4.2), which, in combination with the variation of the wave type in function of the slide type, water body geometry and the location in the water body, are reasons why a clear classification of SLTs is challenging.

2.7. Effect of the water body geometry

2.7.1. Overview

The SLT characteristics highly depend on the water body geometry (Jiang and LeBlond, 1994; Couston et al., 2015; Heller and Spinneken, 2015; Evers et al., 2019b; Ruffini et al., 2019). Most studies have been conducted in 2D at uniform water depth, 3D studies are rarer (Fig. 2, Table 2). The geometry affects the maximum wave already in the generation zone with $H_{3D,M} \leq H_{2D,M}$ and $a_{3D,M} \leq a_{2D,M}$ (Heller et al., 2012; Heller and Spinneken, 2015). The water body geometry more severely affects wave propagation with waves in 3D decaying much faster than in 2D due to lateral energy spread resulting typically in an order of magnitude smaller waves in 3D than in 2D at say $x/h = r/h = 20$ (Huber and Hager, 1997; Heller and Spinneken, 2015; Ruffini et al., 2019). The following sections provide more details about these aspects, mainly for idealised geometries (uniform water depth, straight water body boundaries).

2.7.2. 2D studies

Experiments in 2D (Fig. 2b) are less costly and time consuming and allow for better (visual) access for cameras and measurement systems compared to 3D. 2D geometries, such as narrow water bodies with slide impact in longitudinal direction or full width glacier calving in fjords (Evers et al., 2019b; Ruffini et al., 2019), are rare in the field. However, 2D investigations are important as they provide the upper limit of the wave parameters for diverging geometries, which is often sufficient for hazard assessments.

Russell (1837) may be considered as the first 2D SLT study. His setup consisted of a block impacting vertically into a flume producing a solitary wave (RWG). Many further 2D SLT studies followed (Table 2). They revealed wave height decays in the range $H(x)/h \propto (x/h)^{-1/5}$ to $(x/h)^{-1/2}$ (Eq. (2), Kranzer and Keller, 1959; Law and Brebner, 1968; Wiegel et al., 1970; Huber and Hager, 1997; Heller and Hager, 2010; Heller and Spinneken, 2013). Decays not following a power-law (Kamphuis and Bowering, 1970; Zweifel et al., 2006) are rare. This range of decay laws can be explained with different experimental conditions (different wave types, dispersion, Sections 2.6 and 2.9). Overall representative estimates for 2D SLT decays are $H(x)/h \propto (x/h)^{-1/4}$ and $a(x)/h \propto (x/h)^{-1/4}$.

2.7.3. 3D studies

3D studies are typically conducted in a rectangular basin (Fig. 2c). Theoretically, a wave train from a point source propagates on an open water surface with $(r/h)^{-1.0}$ (Kranzer and Keller, 1959). Deviations from this decay are due to the partially directed slide momentum in the propagation direction for 3D SLTs, propagation on semi-, rather than full-circles, and the non-linear and dispersive nature of SLTs. Nevertheless, decays with an exponent –1.0 were observed by Heller and Spinneken (2015) (Eq. (4)) and Johnson and Bermel (1949) and approximately by Løvholt et al. (2008), Panizzo et al. (2005b) and Heller et al. (2021) (exponents −0.81 to −7/6). Mohammed and Fritz (2012) observed a range of exponents depending on the governing parameters and a slower decay was observed by Huber and Hager (1997) (−2/3). Evers et al. (2019a) and Bregoli et al. (2017) found exponential decays in the far field.

SLTs are largest along the slide axis ($\gamma = 0°$) and decrease with larger/smaller γ. This is typically described with a cosine function such as $\cos^2(2\gamma/3)$ (Eq. (4), Huber and Hager, 1997; Heller et al., 2009; Mohammed and Fritz, 2012; Heller and Spinneken, 2015; Heller et al., 2021). A sech function was used by Evers et al. (2019a) and an exponential function including the cosine function by Panizzo et al. (2005b). The r/h and γ terms are typically combined to a product, complimented with the relevant governing parameters (Eq. 4). Based on the representative 2D and 3D decay laws $(x/h)^{-1/4}$ and $(r/h)^{-1.0}$, respectively, an identical large SLT in the slide impact zone decays to a 10 times smaller wave at $x/h = r/h = 21.5$ in 3D than in 2D.

2.7.4. Link between 3D and 2D

Some studies were aimed at linking the 3D to the 2D wave characteristics to transfer the significantly larger knowledge from 2D to 3D (Table 2). Huber (1980) was the first to conduct both 2D and 3D tests and found that the 2D and 3D waves in proximity of the slide impact deviate little from each other. This finding was further exploited by Huber and Hager (1997) and Heller et al. (2009) to link 3D with 2D waves. Heller and Spinneken (2015) refined this finding based on 18 2D tests repeated in 3D and found a range from $H_{3D,1,M} = 0.37H_{2D,1,M}$ for relatively slow, thin and small slides (small F, *S* and *M*) to $H_{3D,1,M} = 1.0H_{2D,1,M}$ for relatively fast, thick and large slides (large F, *S* and *M*), i.e. the finding of Huber (1980) is only a good approximation for large F, *S* and *M*. Heller and Spinneken (2015) formulated empirical equations to link both the maximum primary 3D wave parameters ($a_{1,M}$, $H_{1,M}$, $T_{1,M}$) and their evolutions with distance (r/h, γ) to the corresponding ones in 2D. The largest difference of a factor of over 15 between $H_{2D,1}$ and $H_{3D,1}$ waves was observed at the largest distance $x/h = r/h = 35$.

2.7.5. Intermediate geometries

Intermediate geometries between 2D and 3D have also been investigated. Heller et al. (2012) investigated a SLT in 2D, 3D and for $\theta = 15$, 30, 45, 60 and 75°, with θ as the water body side angle (Fig. 2c). For $\theta \geq 15°$ the wave amplitudes and heights are much closer to the corresponding waves in 3D than in 2D and waves for $\theta > 30°$ deviate little from the 3D waves for $\gamma = 0°$. This was confirmed by Heller et al. (2016) with SPH simulations for two wave types in 2D, 3D and $\theta = 7.5$, 15, 30 and 45° for $r/h \leq 7.5$. For $\theta = 7.5°$, $H(r/h = 7.5; \gamma = 0°) \approx 0.5H_{2D}(x/h = 7.5)$ and H rapidly approached H_{3D} with increasing θ.

An important relation to quantify the wave height in intermediate geometries is Green's law considering wave energy flux conservation between two sections 1 and 2 (subscripts 1 and 2)

$$H_2 \Big/ H_1 = (h_1/h_2)^{1/4} \left(b_{w,1}/b_{w,2}\right)^{1/2} \tag{7}$$

with the water body width b_w. Chang et al. (1979) showed that Eq. (7) describes the solitary wave height well up to $x/h = 40$ for a uniform water depth $(h_1/h_2)^{1/4} = 1$ and a slightly diverging flume at $\theta = 1.1°$. Synolakis and Skjelbreia (1993) and Heller et al. (2012) showed that Eq. (7) has a limited applicability for solitary or solitary-like waves for larger θ. In these situations, b_w in Eq. (7) should be replaced with the wave front length (Fuchs and Boes, 2010; Heller et al., 2016; Ruffini

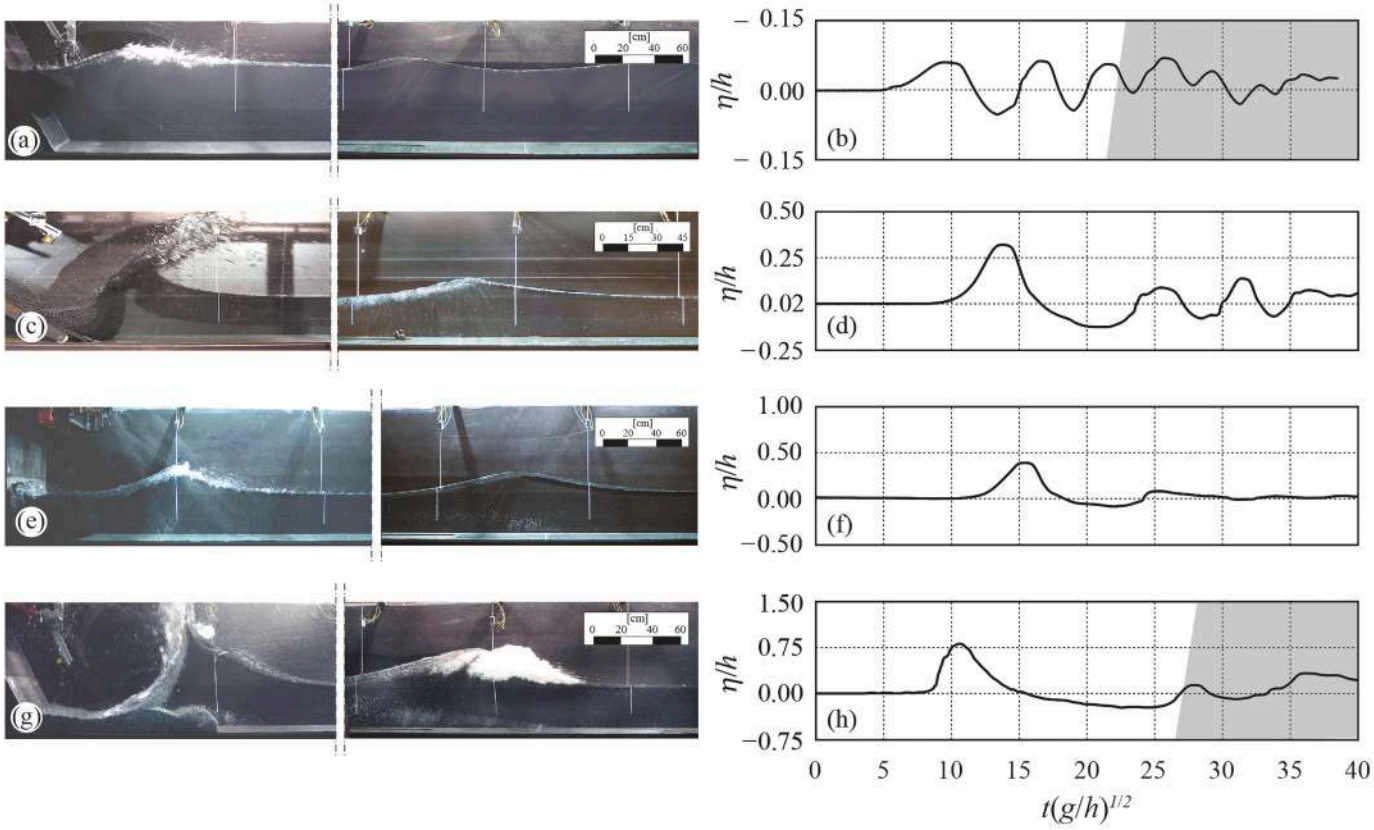

Fig. 6. Generation, propagation and the corresponding free water surface profiles η/h versus $t(g/h)^{1/2}$ of the 4 wave types of SLTs in 2D: (a,b) Stokes-like waves, (c,d) cnoidal-like wave, (e,f) solitary-like wave and (g,h) bore-like wave; the grey areas indicate contaminations due to wave reflection (after Heller and Hager, 2011).

et al., 2019)

$$l_w = b + 2r\theta_{rad} \tag{8}$$

Despite that Eq. (7) applies to shallow water and excludes frequency dispersion, Ruffini et al. (2019) showed with approximate linear, Stokes, cnoidal and solitary waves that Eq. (7) with $b_w = l_w$ is useful to link a and H in the far field of different intermediate geometries and 3D to the corresponding parameters in 2D. Fig. 7(a) illustrates this with H/h for Stokes waves versus r'/h and $\gamma' = 0°$ with the origin ($r' = 0$, $\gamma' = 0°$) located between the near and far field. These wave heights collapse on Green's law prediction in Fig. 7(b) in function of l_w/h. Eq. (7) with $b_w = l_w$ was also instrumental in Ruffini et al. (2019) to collapse all wave data for $0° \leq \gamma' \leq 82.5°$ and to formulate a wave parameter prediction procedure for intermediate and 3D water body geometries based on the 2D wave characteristics in the near field from Heller and Hager (2010).

2.7.6. Other geometries

Slides often impact in lateral direction into a water body (Wang et al., 2017; Tessema et al., 2019; Deng et al., 2020; Zhang et al., 2020; Franco et al., 2021; Liu et al., 2023b; Wang et al., 2023). Whether SLTs can be predicted with the reviewed studies in this Section 2.7 for idealised geometries depends on the reservoir width, i.e. whether the waves have space to fully develop. The parameters x_M of Heller and Hager (2010), r_0 of Evers et al. (2019a) or Δx_g from Xue et al. (2019) are options to estimate the minimum required reservoir width. If this width $\leq x_M$, r_0 and/or Δx_g, then the reservoir width (Wang et al., 2017) should be included as a relevant parameter. However, if this width $> x_M$, r_0 and/or Δx_g, then the reviewed studies in this Section 2.7 may provide good estimates.

Zhang et al. (2020) numerically investigated slides impacting on the side of a basin geometry for wide reservoirs and collected results for the sidewards propagating SLTs (perpendicular to the slide axis) into diverging and converging geometries at angles between 0 and 30°. The decay of a was faster with more diverging geometries. a still decays in converging geometries, but slower than for diverging geometries. Liu et al. (2023b) experimentally investigated a similar configuration with the slide impacting laterally into short and wide trapezoidal 3D geometries. They predicted the 3D wave parameters at the start of the lateral section (perpendicular to the slide axis), with new empirical equations and demonstrated that the waves decay in this lateral section similar as in 2D in Heller and Hager (2010). This confirms that the 3D-2D prediction method postulated in Heller et al. (2009) is suitable for this kind of geometries and that wave reflection from the reservoir boundaries has a small effect on the overall wave decay in the lateral region.

Heller et al. (2012, 2016) investigated the 3D 'corner' case (3Dc) characterised by the slide released in a corner of the water body, inspired by a potential snow avalanche impacting the Küthai reservoir (Fuchs et al., 2011). This 3Dc case resulted in similar waves as for $\theta = 7.5$ or 15°, i.e. significantly larger waves than in 3D. Winckler and Liu (2015) investigated weakly non-linear and weakly dispersive wave propagation along a non-uniform channel with arbitrary cross-section such as the one from Chang et al. (1979). Franco et al. (2021) numerically investigated a slide impacting into 69 idealised mountain lakes combining different lengths (250 to 3000 m), widths (500 to 12000 m) and mean water depths (10 to 100 m). They found a strong correlation of $a(r, \gamma)$ with the 'shape product', a combination of the lake volume, area, width, length and the mean water depth.

A number of case-specific SLT investigations have also been conducted (WCHL, 1970; Davidson and Whalin, 1974; Slingerland and Voight, 1982; Fritz et al., 2001; Løvholt et al., 2008; Fuchs and Boes, 2010; Fuchs et al., 2011; Abadie et al., 2012; BGC, 2012; Lindstrøm et al., 2014; Couston et al., 2015; Gabl et al., 2015; Lüthi and Vieli, 2016; Wang et al., 2016; Gylfadóttir et al., 2017; Tan et al., 2018; Rauter et al., 2022). The link between SLTs in idealised to more complex water body

geometries observed in the field still needs to be fully established and there is also more work required into converging geometries to complement the findings of Winckler and Liu (2015) and Zhang et al. (2020).

2.8. Effect of the non-uniform bathymetry

Nearly all generic SLT studies in Table 2 have been conducted at a uniform h to reduce complexity, as intermediate- and shallow-water waves are affected by a changing h. The focus of this section is on the offshore transformation of SLTs due to a changing h, e.g. at a submerged island, a submarine canyon or a continental shelf step as shown in Fig. 8. Whilst Eq. (7) may be applied to predict the transmitted (subscript t) wave height H_t for mild changes in h, the bathymetric changes are often abrupt and may involve wave breaking, which cannot be considered by Eq. (7).

Some studies investigated wave transmission over low crested structures for water waves in general. Beji and Battjes (1993) used a submerged asymmetric trapezoidal bar with a mild slope and investigated three different types of waves namely non-linear non-breaking waves, spilling breakers and plunging breakers. The waves became asymmetric on the positive slope and the primary wave was followed by a wave train downwave the bar, generated by a process called de-shoaling involving frequency dispersion with frequency components travelling at slightly different speed than the primary wave. Empirical equations to predict transmitted steady wave trains after a submerged structure, such as a rubble mound, were derived by d'Angremond et al. (1997) and Van der Meer et al. (2005). The wave height H_t was thereby expressed in function of the incident wave parameters (e.g. R_c/H_0, with H_0 as the incident (subscript 0) wave height and R_c as the freeboard of the structure) and the underwater feature's characteristics.

A few studies investigated the effect of the non-uniform bathymetry specifically for SLTs (Fig. 8). Fuchs et al. (2010) investigated SLTs running over a trapezoidal obstacle in 2D (Fig. 8c) and measured the wave characteristics up- and downwave of the obstacle. Ruffini et al. (2021) conducted an extensive parameter study in 2D by numerically investigating wave transmission for the full range of SLT types (Section 2.6) over (a) linear beach bathymetries, (b) submerged positive and negative Gaussian bathymetric features (Fig. 8a,b) and (c) submerged positive and negative step bathymetries (Fig. 8d,e). Based on a regression analysis and an ANN, they derived a range of empirical equations for the transformation coefficients a_t/a_0 and H_t/H_0 in function of the incident parameters a_0/H_0, h_f/h_0 and h_f/H_0, with h_f as the water depth at the bathymetric feature (subscript f). A wide range of transformation coefficients between $0.1 \leq H_t/H_0 \leq 1.2$ and $0.2 \leq a_t/a_0 \leq 1.3$ (Figs. 13 and C1 in Ruffini et al., 2021) have been observed.

Based on a limited number of 3D tests, Ruffini et al. (2021) showed that the effects of the geometry (Section 2.7) and non-uniform bathymetry cannot linearly be superimposed for solitary waves propagating over a positive Gaussian bathymetry. Linear superposition may also not apply for other independently investigated parameters affecting SLTs (Section 2.2). This is one of the reasons why the findings of case-specific SLT studies (WCHL, 1970; Davidson and Whalin, 1974; Slingerland and Voight, 1982; Fritz et al., 2001; Løvholt et al., 2008; Fuchs and Boes, 2010; Fuchs et al., 2011; Abadie et al., 2012; BGC, 2012; Lindstrøm et al., 2014; Couston et al., 2015; Gabl et al., 2015; Lüthi and Vieli, 2016; Wang et al., 2016; Gylfadóttir et al., 2017; Tan et al., 2018; Rauter et al., 2022) are difficult to generalise. Further research in the combined effects of the geometry and non-uniform bathymetry, and of effects affecting SLTs in general, is therefore desirable (Section 4.4).

2.9. Frequency domain analysis

Frequency domain analysis methods show that SLTs are a superposition of wave components which may travel at different wave speeds due to dispersion. The associated dispersion of the wave components can temporarily result in a larger a offshore than closer to the slide impact location (Løvholt et al., 2008), as faster wave components overtake slower ones. Whilst most studies (e.g. Huber, 1980; Fritz et al., 2004; Heller and Hager, 2010) analyse the wave speed of the superimposed wave elevation, a frequency domain analysis decomposes SLTs and considers the wave speed of each individual wave (or energy) component.

Panizzo et al. (2002) were the first to apply a frequency domain analysis method (a WT) to SLTs followed by others (Panizzo et al., 2005b; Dong et al., 2010; Mohammed and Fritz, 2012; Heller and Spinneken, 2015; Tang et al., 2018). The WT analysis provides the energy distribution of SLTs over the time-frequency domain as shown in Fig. 9. It is a powerful method to relate the wave celerity to its frequency based on the free water surface time series at one or several locations. Non-dispersive shallow-water waves are characterised by the shallow water wave speed (apart from solitary waves that follow e.g. Eq. (5)), while for dispersive waves each frequency component will propagate with a speed following the appropriate dispersion relation based on the Ursell parameter. Transient waves are often characterised by an intermediate value. In contrast, edge waves propagate with a speed in proximity of the speed given by the dispersion relation of edge waves (Longuet-Higgins, 1967; Romano et al., 2013; Heller and Spinneken, 2015).

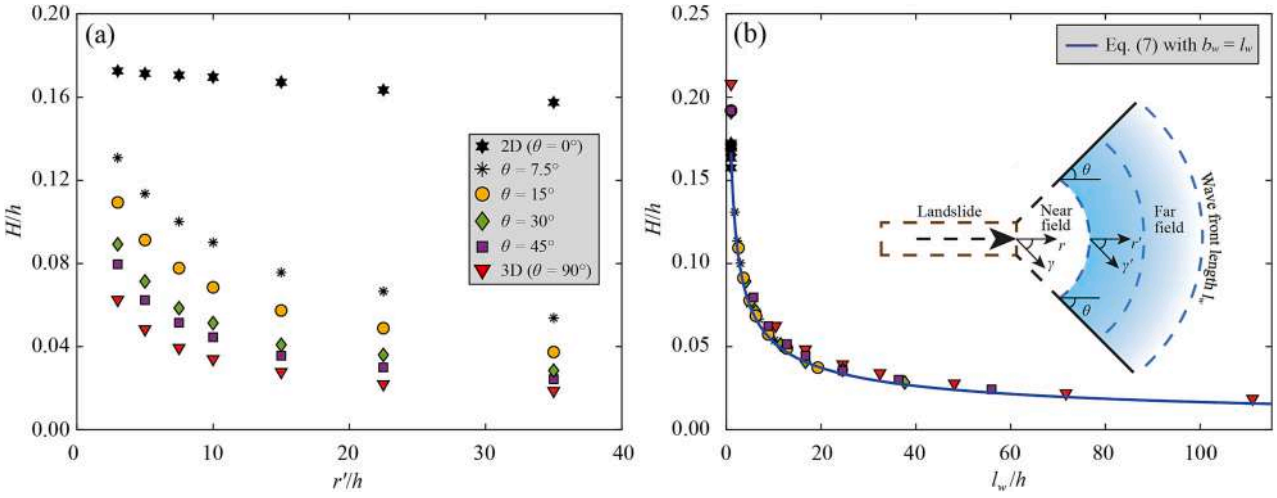

Fig. 7. Relative wave height H/h decay for 5th order Stokes waves in different water body geometries defined with the water body side angle θ in function of (a) the relative radial distance r'/h for $\gamma' = 0°$ and (b) l_w/h compared to Green's law (Eq. (7) with $b_w = l_w$).

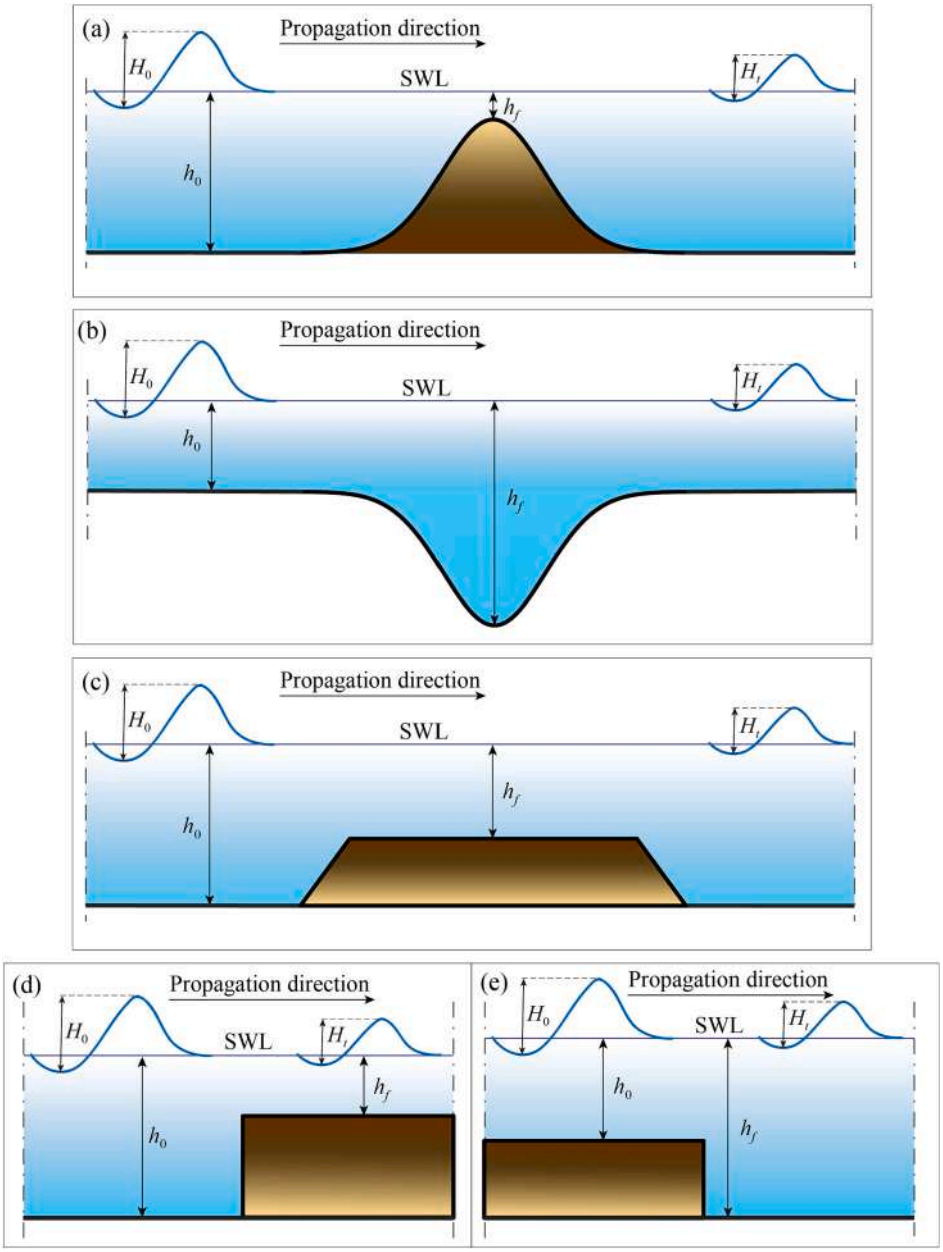

Fig. 8. Sketches of a range of submerged idealised offshore bathymetric features investigated for SLTs including a (a) positive and (b) negative Gaussian bathymetry, (c) submerged trapezoidal and a (d) positive and (e) negative step; (a,b,d,e) were investigated by Ruffini et al. (2021) and (c) by Fuchs et al. (2010); SWL = still water level.

Another frequency domain analysis method suited for SLTs is the wavenumber-frequency (*k-f*) spectral density (or steered response power spectrum) method. This method relies on a spatial array of wave probes (1D, 2D or 3D) and reveals, similar as a WT, at which speed and based on which frequency dispersion relation the waves propagate. Romano et al. (2013) applied this method to SLT propagating around and away from a conical island in laboratory experiments and showed that trapped waves (edge waves) follow the 0^{th} order edge wave mode dispersion relation whilst the offshore waves follow the linear dispersion relation. Bellotti and Romano (2017) developed this work further by applying the Empirical Orthogonal Function method to extract the spatial modes of the wave field. This allows the description of the spatial shape of the wave field and again provides insight into the *k-f* plane representation of the wave energy. Further promising frequency domain analysis methods, the Korteweg-de Vries (KdV, 2D) and Kadomtsev-Petviashvili (KP, 3D) equations in combination with a non-linear Fourier transform (NLFT, Brühl and Becker, 2018; Brühl et al., 2022), will be addressed in Section 4.2.

2.10. Edge waves

Edge waves, also known as lateral onshore wave runup or trapped waves, propagate in 3D along the same slope as the landslide moves (Fig. 10). They are reviewed here as they can exceed the runup height *R* caused by the offshore waves if the landslide slope connects directly to a dam flank or to the shore of interest. Edge waves were investigated for both sloping straight coasts (Ursell, 1952; Lynett and Liu, 2005; Di Risio et al., 2009a; Mohammed and Fritz, 2012; Couston et al., 2015; Heller and Spinneken, 2015; McFall and Fritz, 2016, 2017; Liu et al., 2023a) and conical islands (Di Risio et al., 2009b; Renzi and Sammarco, 2010; Romano et al., 2013; McFall and Fritz, 2016, 2017) such as Stromboli. Some of the underlying physics governing edge waves is different from

offshore propagating SLTs. The edge wave celerity follows approximately the 0th mode of the dispersion relation given by Ursell (1952) (Mohammed and Fritz, 2012; McFall and Fritz, 2017) and they are mainly affected by the slide features, such as b_s, and the hill slope characteristics (Lynett and Liu, 2005). Nevertheless, some studies (Heller and Spinneken, 2015; McFall and Fritz, 2017; Liu et al., 2023a) use h to normalise the edge wave features to be more consistent with the dimensionless parameters used for offshore propagating SLTs (Section 2.2).

Heller and Spinneken (2015) found in 3D for the relative primary SLT amplitude $a_1/h(r/h, \gamma = 0°) \approx 3R_{e,1}/h(r/h, \gamma = 90°)$, with the edge (subscript e) wave runup height R_e, whilst $a_1/h(r/h, \gamma = 73°) \approx 0.82R_{e,1}/h(r/h, \gamma = 90°)$. In other words, R_{e1} is larger than the corresponding offshore wave amplitude at $\gamma = 73°$. They further found $R_{e,1}/h(r/h, \gamma = 90°) \propto (r/h)^{-0.67}$, laying between the 2D and 3D decays of SLTs (Section 2.7). The maximum $R_{e,M}/h$ decays even slower (McFall and Fritz, 2017; Evers et al., 2019b). The maximum runup height $R_{e,M}$ is typically observed for the 2nd or a later wave in the wave train and tends to occur later in the wave train for larger r due to dispersion (Di Risio et al., 2009a, 2009b; Heller and Spinneken, 2015; McFall and Fritz, 2017). $R_{e,M}$ outside the slide path reaches an upper limit (Di Risio et al., 2009b) depending on the experimental conditions and measurement method. Heller and Spinneken (2015) found an upper limit $R_{e,M} \approx 0.15h$ based on wave probes glued to the slope and McFall and Fritz (2017) found $0.25h$ based on still images. Water may runup much higher in the slide path (McFall and Fritz, 2017) as a consequence of the collapsing impact crater (Figs. 3 and 10). $R_{e,M}$ is observed some distance away from the slide impact location, e.g. Di Risio et al. (2009a) observed $R_{e,M}$ at $r \approx 2b_s$, Heller and Spinneken (2015) measured $R_{e,M}$ within $r/h \leq 10$ and McFall and Fritz (2017) at $r \approx 1.23b_s$.

2.11. Analytic achievements

There are different levels on how analytical theories support generic SLT experiments: (i) support of empirical equations, (ii) description of observed wave features and (iii) as a hydrodynamic theory for wave generation and propagation.

Category (i) includes the choice of the dimensionless parameters based on the governing equations (also called inspectional analysis), such as the Euler equations for block slides in Walder et al. (2003) or the mass and momentum conservations based on the mixture theory for granular slides in Zitti et al. (2016). Also part of (i) is Ruffini et al. (2019), who found semi-empirical relations to correlate idealised SLTs in a range of idealised water body geometries in function of Green's law (Eq. (7)).

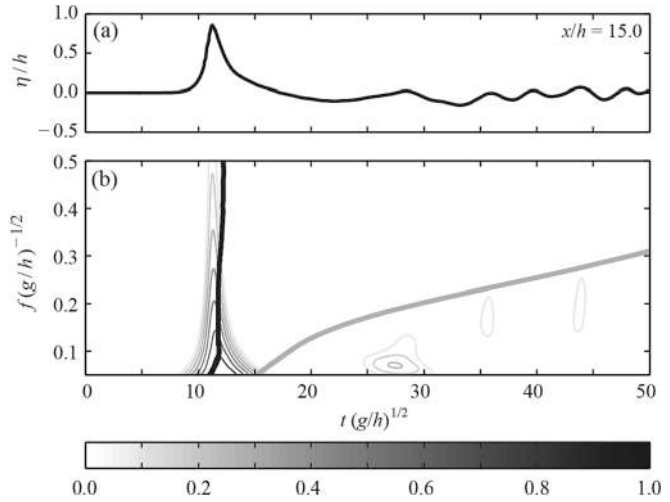

Fig. 9. (a) A 2D SLT train η/h measured at $x/h = 15.0$ resulting in the Wavelet spectra $f(g/h)^{-1/2}$ versus $t(g/h)^{1/2}$ shown in (b). This test involved F = 1.77, S = 0.50 and M = 2.49 and the wave propagation celerity in (b) is represented by (—) Eq. (5) and (—) the linear wave dispersion relation; The energy contained in the primary wave follows Eq. (5), revealing a solitary wave, with later waves following rather linear wave theory (after Heller and Spinneken, 2015).

Category (ii) includes the solitary (Russell, 1837, Eq. (5)) and edge wave theories (Ursell, 1952; Mohammed and Fritz, 2012) to describe the offshore and along-shore SLTs celerity, respectively. Heller et al. (2016) described the SLT kinematics with 5th order Stokes and higher order solitary wave theory. Further, Xue et al. (2019) derived a semi-theoretical equation to describe the free surface profiles of Stokes-like SLTs. Brühl and Becker (2018) decomposed SLTs into linear, Stokes, cnoidal and solitary waves based on the KdV equations (Section 4.2). Zweifel et al. (2004) applied the momentum and mass conservation to predict a_1 in function of the slide characteristics at impact. A related theory was developed by Mulligan and Take (2017) by assuming two scenarios namely a hydrostatic horizontal pressure gradient in the SLT and hydrodynamic conditions. Finally, Sarlin et al. (2021) correlated a for both bores and solitary waves based on the stationary hydraulic jump and solitary wave theory, respectively.

More challenging than (i) and (ii) are hydrodynamic theories (iii). Such theories involve idealised assumptions such as linear wave theory, incompressible and irrotational flow and idealised block slides with either prescribed slide kinematics or by assuming an idealised initial free surface displacement without modelling the slide. Analytic solutions are often only available for asymptotic limits and the equations are solved numerically (Liu et al., 2003; Couston et al., 2015). Waves generated by a local disturbance such as (underwater) explosions motivated pioneering theoretical work. Kranzer and Keller (1959) theoretically studied waves generated by an initial elevation or depression applied on the water surface based on linear wave theory for the far field. Wiegel et al. (1970) presented numerical solutions of this theory and summarised further theories including that of Kajiura (1963). These early theories provide rough estimates for SLTs as they do not model the slide itself, only an idealised initial disturbance, e.g. in function of a sinus curve.

Noda (1970) modelled the wave generation mechanism (also based on linear wave theory and irrotational flow) for both a vertical falling block (RWG) of infinite height (no backflow) and a horizontal moving piston (the spreading case in Fig. 5) by taking the slide movement as a known time-dependent velocity boundary condition into account. The comparison of his solution with a selected experiment of Wiegel et al. (1970) shows a typical agreement of 20% in the far field wave profile for the RWG and a_M/h is approximately 10 to 30% smaller than laboratory observations of non-linear waves. The findings for the piston mechanism by Noda (1970) are related to the wavemaker theory (e.g. Dean and Dalrymple, 2004). The RWG has been revisited by Di Risio and Sammarco (2008) who, in addition to the work of Noda (1970), also model the backflow over the block once it is below the water surface as well as the velocity field generated under the submerging landslide. Again based on linear wave theory, they achieve a remarkably good agreement with laboratory wave profiles in the far field.

More recent studies achieved analytic solutions which remarkable well describe the free water displacements forced by rigid idealised-shaped slides both in the near and far field. Liu et al. (2003) derived a 1D analytical model of waves generated by a moving block on a sloping beach by including the kinematics of the block motion as a forcing term in the linear shallow-water equation. This concept was further developed by Sammarco and Renzi (2008) into a 2-horizontal-dimension (2HD) model to describe the offshore components and the transient edge waves generated by a Gaussian-shaped rigid slide along the shoreline of a plane beach. Renzi and Sammarco (2010) derived a 2HD analytic solution for the same slide type at conic islands, also based on the forced linear shallow-water equation, in combination with the Heun functions (near field with variable h) and the Hankel function (far field with h = constant). Their free surface predictions resulted in an overall good agreement with a SLT experiment of Di Risio et al. (2009b).

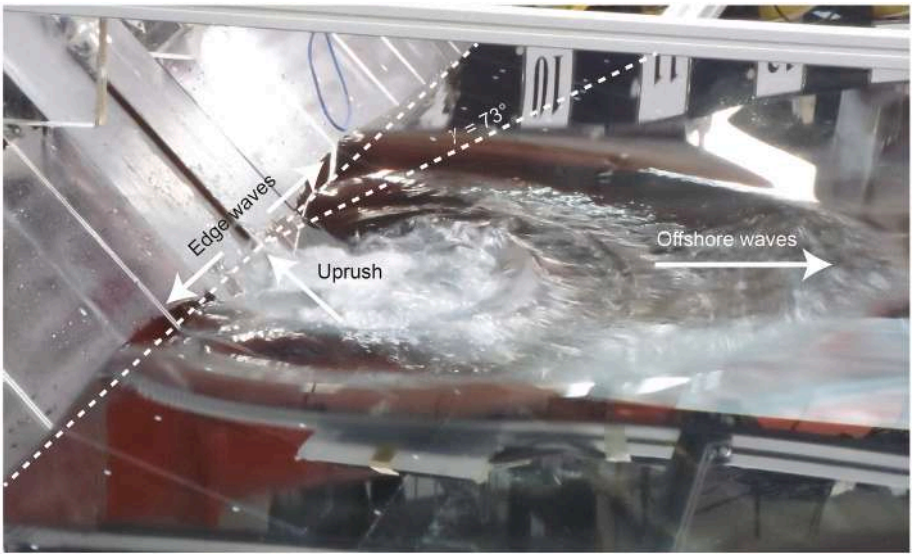

Fig. 10. Landslide-tsunami propagation in 3D from a 45° slope with offshore propagating waves, edge waves and the uprush in the wake of the already submerged landslide (Evers et al., 2019b).

Finally, Renzi and Sammarco (2012) extended the original plane beach model of Sammarco and Renzi (2008) by also considering a more realistic double-parabolic rather than double-Gaussian landslide shape, and by including a semi-plane beach (an initial slope transitioning into a horizontal section) on the wave field. More analytic work is available for long wave propagation and runup (e.g. Synolakis and Skjelbreia, 1993; Winckler and Liu, 2015; Lalli et al., 2019), which is outside of the scope of this review.

3. Gaps and shortcomings in generic empirical equations (approach (I))

3.1. Gaps in approach (I)

The following highlights some key points based on the review in Section 2 along with some research gaps to support approach (I) and SLT hazard assessment until alternative methods, as suggested in Section 4, have reached the necessary maturity to support or replace approach (I).

- Many aspects of SLTs, with sometimes contradicting outcome, have been investigated (Table 2); in general, efforts should be put into the (physical) understanding why different studies provide different outcomes rather than to add more empirical data for already investigated effects (Section 2)
- Whilst a lot of research is available for the effect of the slide type, a limited amount of research has been conducted into the mass movement type (Section 2.4)
- Linking the transferred slide energy directly to a_M or H_M has not been achieved to date as this may be too challenging (Section 2.5)
- The effect of the water body geometry based on real geometries needs to be better understood and related to the already investigated idealised ones (Section 2.7)
- The effects of independently varied parameters on SLTs cannot linearly be superimposed such that more research into the combined effects (e.g. of the geometry and non-uniform bathymetry) is required (Sections 2.7 and 2.8)
- Frequency domain analysis methods are promising and some of them (e.g. KP NLFT for 3D SLTs) have not yet been applied to SLTs (Section 2.9)
- Analytic findings are highly desirable to enhance our physical understanding of SLTs and to improve the longevity of hazard assessment methods (Section 2.11)
- Several of these research gaps may be addressed with support of machine learning (ANN, Section 4.4)

3.2. Shortcomings of approach (I)

A 1st shortcoming of approach (I) in Section 1.1 is that it is unrealistic time and resource intensive to vary all relevant parameters mentioned in Section 2.2 within one study. Most studies varied 4 - 5 or even less parameters. A systematic variation of all 7 dimensionless parameters as well as the slide model (represented by 3 (block slide), 5 (granular slide) and 3 (viscoplastic slide) sub-parameters), mass movement type, water body geometry and bathymetry (Section 2.2) with 3 configurations each results in $3^{13} + 3^{15} + 3^{13} = 17.54$ million experiments. This rough estimate reduces to say 175400 (≈1%) with an Orthogonal Experimental Design (OED) (Wang et al., 2016, 2017, 2018, 2023; Huang et al., 2017; Xue et al., 2019; Li et al., 2023). This number is significantly larger than the 6481 experiments conducted to date (Table 2). It is therefore unrealistic to fully investigate all possible configurations within approach (I).

A 2nd shortcoming of approach (I) is that different studies investigated significantly different dimensionless parameter ranges. This is illustrated with Fig. 11 showing the parameter spaces for F, S, D, B, L_s, V, α and r/h in the 8 major 3D SLT studies from Table 2. Fig. 11(a) includes the 4 block slide studies (including Huang et al., 2014, who also tested granular and mixed slides) and Fig. 11(b) the 4 granular slide studies with some assumptions to add estimates for not available limitations (NA). The maximum values (100%) for each parameter corresponds to the largest investigated value over all 8 studies. These studies range from a vertically dropping rigid block of density lighter than water into 1 m deep water (Heller et al., 2021) to a pneumatically accelerated granular slide with a grain density of 2600 kg/m^3 impacting 0.30 m deep water on a 27.1° slope (Mohammed and Fritz, 2012). The parameters ρ_s and/or α were often kept constant, whilst other dimensionless parameters were investigated in different ranges (e.g. $0 < r/h < 80$ by Mohammed and Fritz (2012) and $0 < r/h < 4.54$ by Huang et al. (2014)).

Table 4 illustrates the results of using the different empirical equations on the prediction for a_M of the 2007 Chehalis case for the 8 3D studies included in Fig. 11. The slide parameters were taken from Evers (2017) complemented with some parameters from other studies as outlined in the caption of Table 4. Huber and Hager (1997) provide an empirical equation for H_M only, for which $a_M = H_M/2$ was assumed in Table 4 (this introduces an estimated error of 30% for the Chehalis case). Panizzo et al. (2005b), Mohammed and Fritz (2012), Heller and

Spinneken (2015) and Evers et al. (2019a) provide an empirical equation for a_1 for which $a_M = a_1$ is assumed (estimated error of 100%). Finally, for Huber and Hager (1997), Panizzo et al. (2005b) and Mohammed and Fritz (2012) a value for r/h, i.e. the location of a_M, is required for which the impact radius $r_0/h = 2.5\{PB\cos[(6/7)\alpha]\}^{1/4} = r/h = 2.80$ from Evers et al. (2019a) was selected, in combination with $\gamma = 0°$.

The predicted a_M vary between 5.9 (Panizzo et al., 2005b) and 256.2 m (Huang et al., 2014). The small value of 5.9 m is most likely due to a spring system used at the slope toe by Panizzo et al. (2005b) stopping the slide masses abruptly and preventing an efficient slide to wave energy transfer (Section 2.5). The large value of 256.2 m is due to a small kinematic friction coefficient $\mu = 0.003$, which is significantly different from the investigated range $\mu = 0.43$ to 0.47 by Huang et al. (2014) (changing μ to 0.43 by keeping all other parameters unchanged would result in $a_M = 162$ m). Huber and Hager (1997), Mohammed and Fritz (2012) and Bregoli et al. (2017) predict $a_M \approx 20$ m. Evers et al. (2019a) ($a_M = 37.0$ m) and Heller et al. (2021) ($a_M = 47.1$ m) predict larger values and the block model study of Heller and Spinneken (2015) an even larger value ($a_M = 57.8$ m). Excluding the unrealistic value from Huang et al. (2014), the discrepancy in predicting a_M is a factor of 57.8/5.9 = 10. This is clearly unsatisfactory and cannot fully be explained by the introduced uncertainties ($a_M = H_M/2$, $a_M = a_1$) or the different slide models (block versus granular slide).

Note that all 8 studies in Table 4 have been conducted in 3D. In general, studies also involve different water body geometries and sizes, measurement systems and investigated different wave parameters (Table 2). These are reasons why predictions with empirical equations from different studies can vary significantly, as illustrated with Table 4 and in previous studies (Fritz et al., 2004; Heller and Hager, 2010; Watt et al., 2012; Heller and Spinneken, 2013, 2015; Evers and Hager, 2016; Bullard et al., 2019a; amongst others). Such discrepancies are a direct consequence of the empiricism of the SLT research discipline and indicate a strong need for a step change.

4. Options for a step change

4.1. Introduction

From a scientific point of view and based on the milestone studies mentioned in Section 2.3, most progress in generic SLT research was achieved approximately 20 years ago. The significant number of studies after 2005 are not reflected in a proportional increase in milestone studies. A step change is therefore required for SLT research based on generic experiments. The following sections introduce into some potential options to initiate this step change.

4.2. Korteweg-de Vries (KdV) and Kadomtsev-Petviashvili (KP) equations

The KdV (for 1D wave propagation, i.e. to describe flume data) and the KP (2D, i.e. for basin data) partial differential equations describe weakly non-linear shallow-water flows. Their solutions can represent the theoretical wave type range from sines, Stokes, cnoidal to solitary waves (Osborne, 2010). The KdV/KP equations in combination with the NLFT are well suited to analyse and describe SLTs as they are typically highly non-linear, intermediate- to shallow-water waves and have indeed been classified as Stokes-, cnoidal- and solitary-like waves (Section 2.6). In contrast to the WT (Panizzo et al., 2002) and the Hilbert-Huang transform (HHT, Dätig and Schlurmann, 2004), the KdV/KP equations combined with the NLFT also consider the important effect of h on the wave profiles and they can explicitly consider non-linear wave-wave interactions (Osborne, 2010; Brühl and Becker, 2018). The superposition of these components and their interactions result in the original wave profile and, crucially, have the potential to reliably predict wave profiles at any desired point in the far field, even bores (Brühl et al., 2022). This is much more challenging for the WT and the HHT (Brühl and Becker, 2018).

Fig. 12 illustrates the potential of the KdV equation based on 2D SLT laboratory wave train data measured at seven positions (Fig. 12a). The decomposed wave train (Fig. 12b) includes one dominant solitary wave. Whilst the superimposed wave amplitude a in the measured laboratory data is decaying, this dominant decomposed solitary wave amplitude $a_{s,1}$ remains essentially constant over all measured positions and beyond. This potentially most dangerous wave component propagates faster and will eventually separate from the wave train in the far field due to frequency dispersion. Generic empirical equations describe SLTs with the superposition of all amplitude components, such that they miss the underlying key-physical processes of SLTs. This results in a dangerous underestimation of the wave magnitude in Fig. 12(b) as the

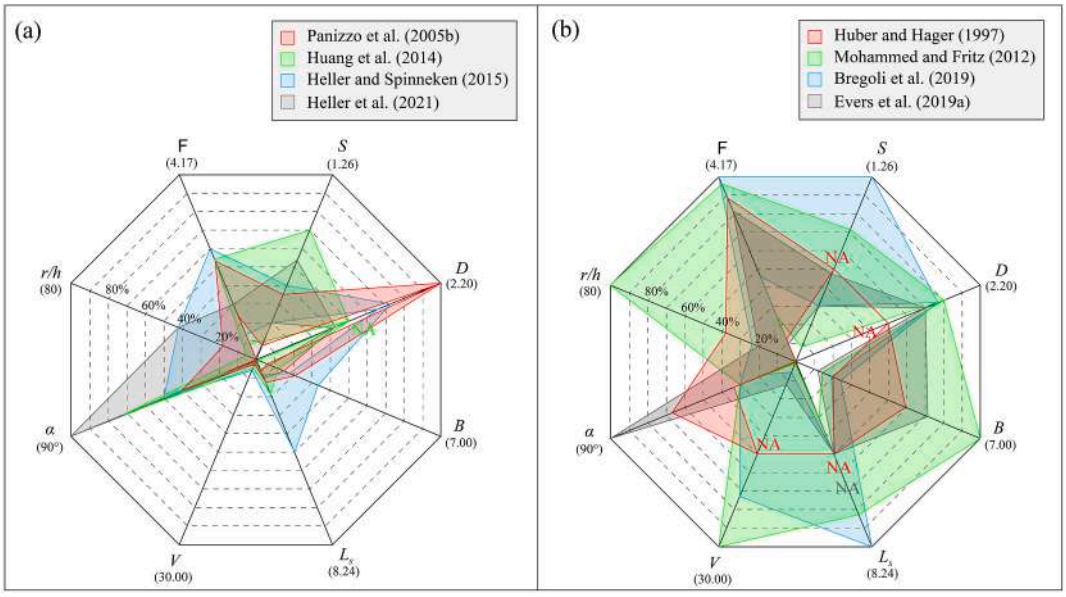

Fig. 11. Parameter spaces for 3D SLT studies illustrating the significantly different parameter limitations: (a) block slide and (b) granular slide studies. The maximum values (100%) correspond to the largest investigated value over all shown 3D studies.

Table 4
Maximum wave amplitude a_M prediction for the 2007 Chehalis case with empirical equations from the major 3D SLT studies included in Fig. 11; The slide parameters are taken from Table 5.4 in Evers (2017) complemented with the slide length $l_s = 375$ m and the porosity $n = 40\%$ (Bregoli et al., 2017), the landslide release height $h_c = 500 + [(840 - 500)/2] = 670$ m based on the maximum and minimum slide release heights from Wang et al. (2015), the relative slide mass $M = 1.64$ based on the values given by Evers (2017) and the kinematic friction coefficient $\mu = 0.003$ (Wang et al., 2015).

Study	Equation	a_M (m)
Huber and Hager (1997) (their Eq. 6)	$\frac{H_M}{2} = a_M = 0.88 sin\alpha \left(\frac{\rho_s}{\rho_w}\right)^{0.25} \left(\frac{V_g}{b_s h^2}\right)^{0.50} \left(\frac{r}{h}\right)^{-2/3} cos^2\left(\frac{2\gamma}{3}\right) h$	23.2
Panizzo et al. (2005b) (their Eq. 13)	$a_1 = a_M = 0.02\left(\frac{b_s s}{h^2}\right)(sin\alpha)^{-0.90}\left[t_s\left(\frac{g}{h}\right)^{0.50}\right]^{-0.27} exp(1.6 cos\gamma)\left(\frac{r}{h}\right)^{-0.80} h$ $t_s\left(\frac{g}{h}\right)^{0.50} = 0.43\left(\frac{b_s s}{h^2}\right)^{-0.27}\left(\frac{V_s}{\sqrt{gh}}\right)^{-0.66}(sin\alpha)^{-1.32}$	5.9
Mohammed and Fritz (2012) (their Eq. 2a)	$a_1 = a_M = 0.31 F^{2.10} S^{0.60}\left(\frac{r}{h}\right)^{\left(-1.2F^{0.25}S^{-0.02}B^{-0.33}\right)} cos\gamma h$	18.5
Huang et al. (2014) (their Eq. 4)	$a_M = 0.667\left(\frac{h_c(1-\mu\, cot\alpha)}{h}\right)^{0.334}\left(\frac{b_s}{s}\right)^{0.754}\left(\frac{l_s}{s}\right)^{0.506}\left(\frac{s}{h}\right)^{1.631} h$	256.2
Heller and Spinneken (2015) (Eq. 3 or their Eq. 4)	$a_1 = a_M = 0.50\left(FS^{1.10}M\right)^{0.85} h$	57.8
Bregoli et al. (2017) (their Eq. 14)	$a_M = 0.118\left(\frac{s}{h}\right)^{0.459}\left(\frac{l_s}{h}\right)^{0.463} F^{0.554} h$	19.8
Evers et al. (2019a) (their Eq. 9)	$a_1 = a_M = 0.20 P^{0.50} B^{0.75}\{cos[(6/7)\alpha]\}^{0.25} h$	37.0
Heller et al. (2021) (their Eq. B2, gravity-dominated fall)	$a_M = 0.13\left(E_r^{0.20} F^{1.66} S^{0.21} B^{1.46} V^{0.20} D^{0.20}\right)^{0.50} h$ with $E_r = \left[b_s \rho_s g s l_s\left(h_c + \frac{l_s \rho_s}{2\rho_w} - \frac{l_s}{2}\right)\right] \Big/ \left(h^4 g \rho_w\right)$	47.1

superimposed a is smaller than the individual decomposed component $a_{s,1}$ both at the encircled point and further downwave.

A limited amount of research has been conducted with the KdV equations in SLTs and, to the authors knowledge, the KP NLFT method has not yet been applied to SLTs. The KdV/KP equations in combination with the NLFT have therefore the genuine potential to provide a step change in SLT characterisation and prediction, and in other wave phenomena, through new physical insight and the consideration of up to now neglected dominant wave components.

4.3. Generally applicable numerical code

Numerical models, in contrast to generic empirical equations, can consider complex slide scenarios, slide rheologies, water body geometries and topographies. State of the art mathematical models and methods with promising results include the Discrete Element Method (DEM, e.g. Shan and Zhao, 2014), depth-averaged equations (e.g. Savage-Hutter model, e.g. Ma et al., 2015) and various (fluid-like) rheologies (Newtonian, Bingham, Coulomb, Voellmy, Herschel-Bulkley, etc.) for slide propagation (e.g. Yavari-Ramshe and Ataie-Ashtiani, 2016). Navier-Stokes Equations (NSEs) based models (Direct Numerical Simulation, Large Eddy Simulations (LES), RANS equations) are suitable for wave generation (e.g. Liu et al., 2005; Heller et al., 2016; Chen et al., 2020; Rauter et al., 2022). For wave propagation, numerical models based on the non-hydrostatic non-linear shallow-water equations (NH-NLSWEs, e.g. Ruffini et al., 2021; Zijlema et al., 2011), the Boussinesq-type equations (e.g. Kim et al., 2009; Shi et al., 2012; Tehranirad et al., 2015) and potential flow equations (e.g. Huang et al., 2013) are often used. Fig. 13 shows numerical examples for wave generation (RANS equations) and propagation (NH-NLSWEs). Depending on the complexity and desired output parameters, wave runup and inundation may be modelled with the same approaches as wave propagation (e.g. NH-NLSWEs) or higher level approaches similar as for wave generation (e.g. RANS equations).

Such models are implemented in a range of codes and solvers including CFDEM (e.g. Shan and Zhao, 2014), DualSPHysics (e.g. Heller et al., 2016), OpenFOAM (e.g. Rauter et al., 2022), FLOW-3D (e.g. Franco et al., 2021), ANSYS Fluent (e.g. Xing et al., 2016), REEF3D (e.g. Kamath et al., 2017), THETIS (e.g. Tehranirad et al., 2015), NHWAVE (e.g. Grilli et al., 2019), GERRIS (e.g. Viroulet et al., 2013a), Fluidity (e.g. Smith et al., 2016), FUNWAVE-TVD (e.g. Tehranirad et al., 2015), Coulwave (e.g. Lynett et al., 2014), GeoClaw (e.g. Kim et al., 2017) or SWASH (Fig. 13b, e.g. Ruffini et al., 2021). Some further successes for SLT simulations have been achieved with the Tsunami Square method (e.g. Wang et al., 2019a), the Immersed Boundary Method (Fig. 13a, e.g. Chen et al., 2020), the Particle Finite Element Method (e.g. Mulligan et al., 2020) and the Lattice Boltzmann method (e.g. Qiu et al., 2019).

Caution is required in applying the appropriate model for the specific processes, e.g. whilst the NH-NLSWEs are appropriate for wave propagation in the far field, they may be inappropriate for SLT generation. Publications older than say 10 years should be read in the context of the available (computer) resources at that time as then acceptable compromises may be inacceptable nowadays. For example, advances in computer resources (Central Processing Units (CPUs) parallelisation, Graphics Processing Units (GPUs) utilisation and parallelisation, Macías et al., 2021) make it more and more difficult to justify the application of the linear shallow-water equations for SLT propagation as key physical processes, such as frequency dispersion (Glimsdal et al., 2013), cannot be modelled. On the other hand, the simulation of wave propagation in a large water body with say the RANS equations is currently challenging due to excessive computational cost and numerical dissipation (Violeau and Rogers, 2016).

Various methods and codes are designed for specific SLT conditions and scenarios for which they typically provide good results (Chen et al., 2020; Grilli et al., 2019; Rauter et al., 2022). However, this often involves prescribed rather than resolved slide motion (e.g. Ataie-Ashtiani and Yavari-Ramshe, 2011), parameter fittings and optimisations based on laboratory experiments (e.g. Heller et al., 2016), predicting parts of

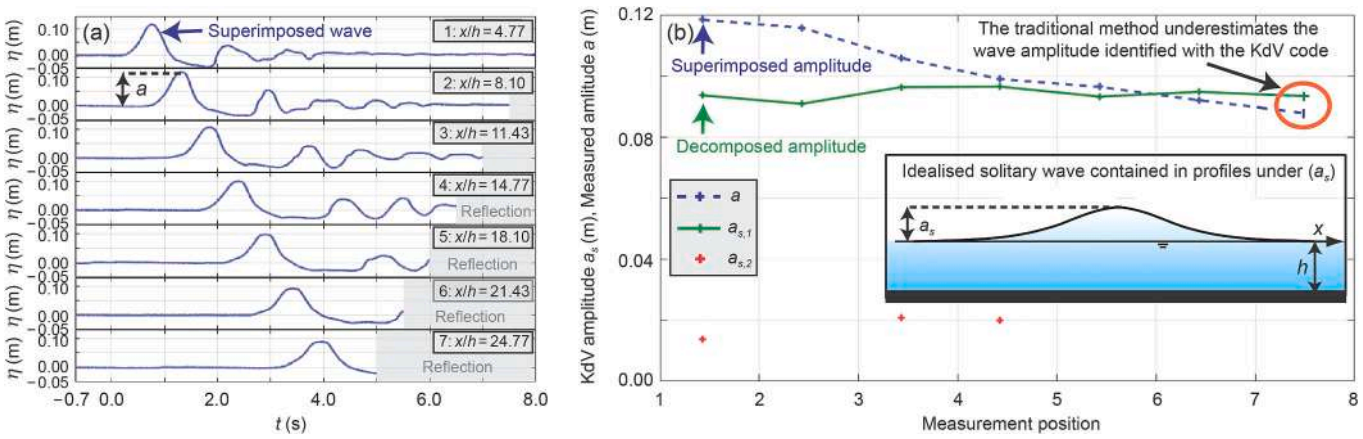

Fig. 12. (a) SLT profiles η (m) versus time t (s) measured at 7 distances from the slide impact in 2D (Heller and Spinneken, 2015) and (b) wave amplitudes a together with the primary $a_{s,1}$ and secondary solitary wave amplitude $a_{s,2}$ identified by the NLFT in the data in (a) (after Brühl and Becker, 2018).

the phenomena only (e.g. the near field in Liu et al., 2005) and ad hoc assumptions (e.g. rigid slide motion in Chen et al., 2020) making reliable predictions of future events challenging. To the authors knowledge, no currently available single model would be able to predict the full range of SLT scenarios shown in Tables 1 and 2 with confidence. The development of a reliable generally applicable numerical code able to provide realistic results over the full range of SLT scenarios would be valuable. This would likely involve the coupling of the different approaches for slide propagation, wave generation, wave propagation, runup and inundation (Abadie et al., 2012; Yavari-Ramshe and Ataie-Ashtiani, 2016; Tan et al., 2018). Such a code further involves challenges such as computational cost, calibration and validation for a wide range of SLT scenarios based on laboratory benchmark tests (see validation tests 7, 11 and 15 on https://spheric-sph.org/validation-tests, Liu et al., 2005; Fuchs et al., 2010; Mohammed and Fritz, 2012; Romano et al., 2016) and past cases (Table 1), importing and handling topographic and bathymetric data. Open source computational environments such as OpenFOAM (https://openfoam.com), including its forks, and DualSPHysics (https://dual.sphysics.org, Domínguez et al., 2022) already advance in this direction, but significantly more work is required. Prototype-specific numerical modelling of SLTs will most likely be key for advancing the field of SLTs by more actively using laboratory data for validation.

4.4. Machine learning

Machine learning (ML) is of increasing importance in water wave mechanics (James et al., 2018) and fluid mechanics in general (Brunton et al., 2020). ML is data driven such that it may not provide new insight into the underlying physics of SLTs. However, ML may be a valuable tool to support SLT hazard assessment and research by improving and optimising empirical predictions. Panizzo et al. (2005b) pioneered the application of ML in SLTs followed by Meng et al. (2020) and Ruffini et al. (2021). These studies relied on ANN to derive optimised correlations for individual wave parameters, including a_M, H_M and the transmitted wave parameters downstream of a bathymetric feature, as an alternative to regression analyses. Wu et al. (2022) applied more advanced ML techniques in the form of a physics-informed neural network (PINN). They replicated the RWG experiments of Monaghan and Kos (2000) in the entire domain by minimising errors between water particle velocities predicted by the neural network and the ones satisfying mass and momentum conservation. Feng et al. (2022) applied a random forest model to predict entire wave profiles of a priori known wave types. However, the full potential of ML in SLTs has not yet been exploited.

Although the maximum wave characteristics a_M and H_M are relevant in many situations, the transformation of the maximum waves with distance from the slide impact location are more important as the endangered structures are normally not at the location where a_M or H_M is observed. The description of $a(x)$, $a(r, \gamma)$, $H(x)$ or $H(r, \gamma)$ requires e.g. sequence modelling (Géron, 2019) capturing and processing data over a sequence of times or distances. Further, also classifications (wave type) have only recently been exploited for SLTs (Jenkins et al., 2023). The potential of PINN is also significant as it may be used to predict the slide

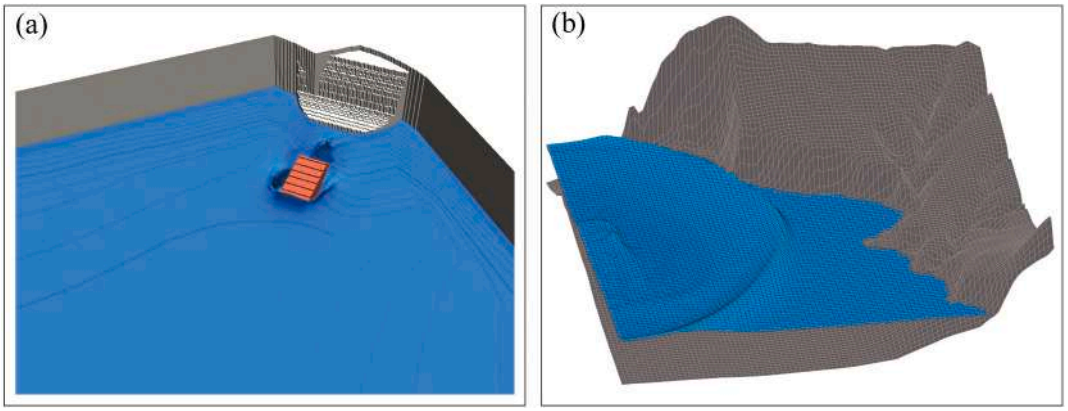

Fig. 13. Numerical SLT simulation examples involving natural bathymetries: (a) Generation of the 2014 Eqip Sermia case with the natural initial iceberg geometry modelled with the Immersed Boundary Method and the RANS equations in Foam-extend (courtesy of Dr. Fan Chen) and (b) propagation of a hypothetical SLT originating from Es Vedrà, offshore Ibiza, modelled with the NH-NLSWEs in SWASH.

kinematics and hydrodynamics in the entire domain. This could be based on a combined approach involving laboratory and numerical results, governing equations and ML. There are many further ML techniques available for the investigation of SLTs.

A multiple regression analysis can be challenging, particular for SLTs depending on approximately 14 independent parameters (Sections 2.2 and 3.2). On the other hand, 14 input variables is a low number for ML which can involve a few millions of variables in computer vision/medical imaging. Table 2 shows that over 6000 generic SLT experiments have been conducted to date. If a large part of these experiments could be made available, then universal data-driven empirical equations for SLTs may be derived based on ML, combining the full parameter ranges and experimental conditions included in Table 2. This would be superior to empirical equations based on individual data sets (Tables 2 and 4) and likely result in more reliable predictions.

5. Conclusions

Subaerial landslide-tsunamis (SLTs) are generated by various mass movements in a range of water bodies. Past SLTs reached runup heights of over half a kilometre and resulted, in combination with associated phenomena and tsunamis generated by partially submerged landslides, in a cumulative death toll in excess of 58000. Essentially 5 approaches, and combinations, are available to predict and deal with SLTs and to support a more holistic method such as a probabilistic tsunami hazard and risk analysis: (I) generic empirical equations from laboratory and numerical tests, (II) prototype-specific physical model tests, (III) protype-specific numerical model tests, (VI) empirical equations derived from field data and (V) analytical investigations. This article reviewed research into the generation and propagation of SLTs with a particular focus on 76 studies, involving 6481 experiments, contributing to approach (I), i.e. studies intended to predict SLTs for a range of scenarios. This approach is particularly important for an efficient and inexpensive preliminary SLT hazard assessment for situations such as creeping landslides in proximity of a water body, for the planning and operational phases of hydropower dams (Evers et al., 2019b) and as part of a probabilistic tsunami hazard analysis.

A range of past SLT cases were presented in this article and the relevant parameters affecting SLTs were reviewed. Further, the findings of several key areas in SLT research were addressed: the effects of the mass movement type and slide model, slide to wave energy transfer, wave types, the effects of the water body geometry and non-uniform bathymetry, frequency domain analysis, edge waves and analytic achievements. Research gaps and shortcomings around generic empirical equations were also highlighted.

Despite of the progress in all reviewed key areas, the experimental research field of SLTs has in-sufficiently advanced over the last 2 decades. Most milestone studies were published approximately 20 years ago (Section 2.3) and the significant number of generic studies after 2005 (Table 2) are not reflected in a proportional increase in milestone studies. In addition, a significant wave amplitude prediction discrepancy of an order of magnitude between wave basin studies has been illustrated with the 2007 Chehalis case. A step change in generic SLT research is therefore needed. In the 2nd part of this review article, the following potential options to initiate and contribute to this step change were suggested:

Korteweg-de Vries (KdV)/Kadomtsev-Petviashvili (KP) equations: These differential equations describe weakly non-linear shallow-water flows, i.e. they take the effect of the water depth on SLTs into account. They further consider the theoretical wave type range from sines, Stokes, cnoidal to solitary waves. The KdV/KP, in combination with a non-linear Fourier transform, are therefore well suited to describe SLTs. The pioneer study of Brühl and Becker (2018) for flume data provided surprising new physical insight into SLTs including a dominant solitary wave exceeding the superimposed wave amplitude commonly applied in approach (I).

A generally applicable numerical code: In general, numerical simulations, if carefully calibrated and validated, provide more accurate results than generic empirical equations as they can consider complex slide scenarios, slide rheologies, water body geometries and topographies. A significant amount of numerical work into SLTs has been conducted based on various methods and codes designed for specific SLT conditions and scenarios for which they typically provide good results. The development of a reliable generally applicable numerical code, able to provide good results over the full range of SLT scenarios with confidence, would be valuable as prototype-specific numerical modelling of SLTs is increasingly relevant for SLT research and hazard assessment.

Machine learning (ML): ML is data driven and may therefore be a valuable tool to support SLT hazard assessment and research e.g. by improving approach (I). There are many more ML techniques available for SLTs, next to already applied artificial neural networks (Panizzo et al., 2005b; Ruffini et al., 2021), including sequence modelling, classifications and physics-informed neural network (PINN). ML may also be used to derive universal data-driven empirical equations based on all approximately 14 relevant independent parameters for SLTs (Section 2.2) and the 6481 available SLT experiments (Table 2).

Promising for a SLT research step change are also combined approaches, e.g. high-quality laboratory data and field observations can be used for the calibration and validation of generally applicable numerical codes or PINN may combine ML and governing equations with laboratory and numerical data.

Notation

a	wave amplitude, m;
a_s	solitary wave amplitude, m;
A	cross-sectional area of the slide, m^2;
b	flume width, m;
b_s	slide width, m;
b_w	water body width, m;
B	relative slide width;
c	wave celerity, m/s;
d_g	grain diameter, m;
D	relative slide density;
E_{kin}	kinetic wave energy, kgm^2/s^2;
E_{pot}	potential wave energy, kgm^2/s^2;
E_r	relative released energy;
E_s	slide energy, kgm^2/s^2;
E_s'	slide energy per unit width, kgm/s^2;
f	frequency, 1/s;
F	slide Froude number;
g	gravitational acceleration, m/s^2;
h	still water depth, m;
h_c	landslide release height, m;
H	wave height, m;
k	permeability coefficient, m/s; wavenumber, 1/m;
l_s	slide length, m;
l_w	wave front length, m;
L	wavelength, m;
L_s	relative slide length;
m_s	slide mass, kg;
M	relative slide mass;
n	bulk slide porosity, %;
P	impulse product parameter;
r	radial distance, m;
r_0	impact radius, m;
r'	radial distance from the interface between the near and far field, m;
R	runup height, m;
R	Reynolds number;
R_c	freeboard of a structure, m;
s	slide thickness, m;

S	relative slide thickness;
t	time, s;
T	wave period, s;
U	Ursell parameter;
V	relative slide volume;
V_s	slide impact velocity, m/s;
$\forall_g$	grain slide volume, m^3;
$\forall_s$	bulk slide volume, m^3;
W	Weber number;
x	streamwise distance, m;
x_M	streamwise distance of a_M, m;
z	vertical coordinate, m;
α	slide impact angle, i.e. hill slope angle, °;
γ	wave propagation angle, °;
γ '	wave propagation angle from the interface between the near and far field, °;
Δx_g	length of the wave generation zone, m;
η	water surface elevation, m;
θ	water body side angle, °;
θ_{rad}	water body side angle, radians;
μ	kinematic friction coefficient;
ν_w	kinematic viscosity of water, m^2/s;
ρ_g	grain density, kg/m^3;
ρ_s	bulk slide density, kg/m^3;
ρ_w	water density, kg/m^3;
σ_w	surface tension, kg/s^2; and
ϕ	slide front angle, °

Subscripts

e	edge;
f	feature;
M	maximum;
t	transmitted, trough;
0	incident;
1	primary; section 1;
2	secondary; section 2;
2D	two-dimensional (flume); and
3D	three-dimensional (basin)

Superscripts

c	crest; and
1	primary

Abbreviations

ANN	artificial neural network;
CPU	central processing unit;
DEM	discrete element method;
GPU	graphics processing unit;
HHT	Hilbert-Huang transform;
KdV	Korteweg-de Vries;
KP	Kadomtsev-Petviashvili;
LES	large eddy simulation;
ML	machine learning;
MM	mathematical model;
NA	not available;
NH-NLSWE	non-hydrostatic non-linear shallow-water equation;
NLFT	non-linear Fourier transform;
NM	numerical model;
NSE	Navier-Stokes equation;
OED	orthogonal experimental design;
PINN	physics-informed neural network;
PIV	particle image velocimetry;
RANS	Reynolds-averaged Navier-Stokes;
RWG	Russell's wave generator;
SLT	subaerial landslide-tsunami;
SPH	smoothed particle hydrodynamics;
SWL	still water level;
WT	wavelet transform;
1D	one-dimensional;
2D	two-dimensional (flume);
2HD	two-horizontal-dimension;
3D	three-dimensional (basin); and
3Dc	three-dimensional (basin) corner

CRediT authorship contribution statement

Valentin Heller : Conceptualization, Formal analysis, Investigation, Methodology, Project administration, Resources, Validation, Visualization, Writing – original draft, Writing – review & editing. **Gioele Ruffini :** Data curation, Formal analysis, Investigation, Methodology, Resources, Validation, Visualization, Writing – original draft, Writing – review & editing.

Declaration of Competing Interest

The authors declare that they have no known competing financial interests or personal relationships that could have appeared to influence the work reported in this paper.

Data availability

Data will be made available on request.

Acknowledgement

This article is dedicated to Mr Muhammad Awais Zaman, who passed away whilst working on his thesis on SLTs. VH would like to express his gratitude to Prof. emeritus Willi H. Hager for introducing him to the field of SLTs. Further thanks go to the following collaborators: Dr. Sazeda Begam, Prof. Robert M. Boes, Dr. Riccardo Briganti, Dr. Markus Brühl, Dr. Xuexue Chen, Dr. Ben Constance, Dr. Frederic M. Evers, Prof. Hermann M. Fritz, Dr. Helge Fuchs, Dr. Roman Gabl, Dr. Johan Gaume, Dr. Archontis Giannakidis, Dr. Andreas Huber, Prof. emeritus Hans-Erwin Minor, Dr. Panos Psimoulis, Prof. Benedict D. Rogers, Dr. Ashim Sattar, Dr. Johannes Spinneken, Prof. Peter J. Talling, Dr. Savvas Triantafyllou, Dr. Barbara Turnbull, Dr. Sebastian Watt, Dr. Guido Wolters and Dr. Andreas Zweifel. The following PhD and MPhil students contribute(d) to SLT research: Tommaso Attili, Dr. Fan Chen, Zhiwen Chen, David G. Jenkins, Dr. Matthew Kesseler, Jizhixian Liu, Dr. Hai Tan and Muhammad Awais Zaman (1995-2023). The following MSc, undergraduate and exchange students are acknowledged for their interest in SLTs and contributions: Rorik Adams, Mark Bruggemann, Elsa Büchner, Francine Amy Capon, Kelvin Ping Han Chua, Matthew Cobbold, Daniel Fox, Ramandeep Kaur, Robert Kinnear, Jiazhang Liu, Mahtab Moalemi, Annabel Murley, Jamie Nicholson, Jagdeep Singh Powar, Sangchu Quan, Ewan Sloan, Patrick Toone, Cai Yang, Sheng Yang, Runda Zhao and Yifeng Zheng. GR would like to thank Prof. Paolo De Girolamo for the fundings provided for his postdoctoral position at the Sapienza University of Rome. The authors would also like to thank the Editor and two anonymous reviewers for helpful suggestions to improve this article. Some of the reviewed work of the authors has been supported by the China Scholarship Council, the European Community's Horizon 2020 research and innovation programme through HYDRALAB+, contract no. 654110, an Imperial College Research Fellowship (cohort 2011), the Leverhulme Trust, the Natural

Environment Research Council (grant number NE/K000578/1), Nottingham Trent University, a NVIDIA GPU Grant (NVIDIA Corporation), the Swiss Federal Office of Energy (SFOE), the Swiss National Science Foundation (grant no. 200020-103480/1) and the University of Nottingham new lecturer PhD studentship (PhD study of GR).

References

Abadie, S.M., Harris, J.C., Grilli, S.T., Fabre, R., 2012. Numerical modeling of tsunami waves generated by the flank collapse of the Cumbre Vieja Volcano (La Palma, Canary Islands): Tsunami source and near field effects. J. Geophys. Res. 117, C05030.

Ataie-Ashtiani, B., Malek Mohammadi, S., 2007. Near field amplitude of subaerial landslide generated waves in dam reservoirs. Dam Eng. 17 (4), 197–222.

Ataie-Ashtiani, B., Nik-Khah, A., 2008. Impulsive waves caused by subaerial landslides. Environ. Fluid Mech. 8, 263–280.

Ataie-Ashtiani, B., Yavari-Ramshe, S., 2011. Numerical simulation of wave generated by landslide incidents in dam reservoirs. Landslides 8, 417–432.

Attili, T., Heller, V., Triantafyllou, S., 2021. A numerical investigation of tsunamis impacting dams. Coast. Eng. 169, 103942.

Behrens, J., Løvholt, F., Jalayer, F., Lorito, S., Salgado-Gálvez, M.A., Sørensen, M., Abadie, S., Aguirre-Ayerbe, I., Aniel-Quiroga, I., Babeyko, A., Baiguera, M., Basili, R., Belliazzi, S., Grezio, A., Johnson, K., Murphy, S., Paris, R., Rafliana, I., De Risi, R., Rossetto, T., Selva, J., Taroni, M., Del Zoppo, M., Armigliato, A., Bures, V., Cech, P., Cecioni, C., Christodoulides, P., Davies, G., Dias, F., Bayraktar, H.B., González, M., Gritsevich, M., Guillas, S., Harbitz, C.B., Kanoglu, U., Macías, J., Papadopoulos, G.A., Polet, J., Romano, F., Salamon, A., Scala, A., Stepinac, M., Tappin, D.R., Thio, H.K., Tonini, R., Triantafyllou, I., Ulrich, T., Varini, E., Volpe, M., Vyhmeister, E., 2021. Probabilistic tsunami hazard and risk. Analysis: A review of research gaps. Front. Earth Sci. 9, 628772.

Beji, S., Battjes, J., 1993. Experimental investigation of wave propagation over a bar. Coast. Eng. 19 (1), 151–162.

Bellotti, G., Romano, A., 2017. Wavenumber-frequency analysis of landslide-generated tsunamis at a conical island. Part II: EOF and modal analysis. Coast. Eng. 128, 84–91.

BGC, 2012. Mitchell Pit Landslide Generated Wave Modelling. BGC Engineering Inc., Vancouver, BC, Canada. Appendix 4-E.

Bougouin, A., Paris, R., Roche, O., 2020. Impact of fluidized granular flows into water: Implications for tsunamis generated by pyroclastic flows. J. Geophys. Res.-Sol. Earth 125, e2019JB018954.

Boussinesq, J., 1872. Théorie des ondes et des remous que se propagent le long d'un canal rectangulaire horizontal, en communiquant au liquid contenu dans ce canal des vitesses sensiblement pareilles de la surface au fond. J. Math. Pures Appl. 17 (2), 55–108 (in French).

Bregoli, F., Bateman, A., Medina, V., 2017. Tsunamis generated by fast granular landslides: 3D experiments and empirical predictors. J. Hydraul. Res. 55 (6), 743–758.

Bregoli, F., Median, V., Bateman, A., 2020a. The energy transfer from granular landslides to water bodies explained by a data-drive, physics-based numerical model. Landslides 18, 1337–1348.

Bregoli, F., Median, V., Bateman, A., 2020b. Versatile image-based measurements of granular flows and water wave propagation in experiments of tsunamis generated by landslides. J. Vis. 23, 299–311.

Brühl, M., Becker, M., 2018. Analysis of subaerial landslide data using nonlinear Fourier transform based on Korteweg-deVries equation (KdV-NLFT). J. Earthq. Tsunami 12 (2), 1840002.

Brühl, M., Ujvary, S., Barranco, I., Prins, P.J., Wahls, S., Liu, P.L.-F., 2022. Comparative analysis of bore propagation over long distances using conventional linear and KdV-based nonlinear Fourier transform. Wave Motion 111, 102905.

Brunton, S.L., Noack, B.R., Koumoutsakos, P., 2020. Machine learning for fluid mechanics. Annu. Rev. Fluid Mech. 52, 477–508.

Buckingham, E., 1914. On physically similar systems – Illustrations of the use of dimensional equations. Phys. Rev. 4, 345–376.

Bukreev, V.I., Gusev, A.V., 1996. Gravity waves generated by a body falling onto shallow water. J. Appl. Mech. Tech. Phy. 37 (2), 224–231.

Bullard, G.K., Mulligan, R.P., Carreira, A., Take, W.A., 2019a. Experimental analysis of tsunamis generated by the impact of landslides with high mobility. Coast. Eng. 152, 103538.

Bullard, G.K., Mulligan, R.P., Take, W.A., 2019b. An enhanced framework to quantify the shape of impulse waves using asymmetry. J. Geophys. Res.-Oceans 124, 652–666.

Carrier, W.D., 2003. Goodbye, Hazen; Hello, Kozeny-Carman. J. Geotech. Geoenviron. 129 (11), 1054–1056.

Chang, P., Melville, W.K., Miles, J.W., 1979. On the evolution of a solitary wave in a gradually varying channel. J. Fluid Mech. 95, 401–414.

Chen, F., Heller, V., Briganti, R., 2020. Numerical modelling of tsunamis generated by iceberg calving validated with large-scale laboratory experiments. Adv. Water Resour. 142, 103647.

Choi, B.H., Pelinovsky, E., Kim, K.O., Lee, J.S., 2003. Simulation of the trans-oceanic tsunami propagation due to the 1883 Krakatau volcanic eruption. Nat. Hazards Earth Syst. Sci. 3, 321–332.

Clous, L., Abadie, S., 2019. Simulation of energy transfers in waves generated by granular slides. Landslides 16 (9), 1663–1679.

Couston, L.A., Mei, C., Alam, M.R., 2015. Landslide tsunamis in lakes. J. Fluid Mech. 772, 784–804.

Cruden, D.M., Varnes, D.J., 1996. Landslide types and processes. Landslides, special report 247. In: Turner, I., Schuster, A. (Eds.). Transportation Research Board, Washington DC, pp. 36–75.

Dahl-Jensen, T., Larsen, L.M., Pedersen, S.A.S., Pedersen, J., Jepsen, H.F., Pedersen, G., Pedersen, G., Nielsen, T., Pedersen, A.K., Von Platen-Hallermund, F., Weng, W., 2004. Landslide and tsunami 21 November 2000 in Paatuut, West Greenland. Nat. Hazards 31 (1), 277–287.

d'Angremond, K., Van Der Meer, J.W., De Jong, R.J., 1997. Wave transmission at low-crested structures. Coast. Eng. 1996, 2418–2427.

Das, M.M., Wiegel, R.L., 1972. Waves generated by horizontal motion of a wall. J. Waterway. Harbour. Coast. Eng. Div. ASCE 98 (WW1), 49–65.

Dätig, M., Schlurmann, T., 2004. Performance and limitations of the Hilbert-Huang transformation (HHT) with an application to irregular water waves. Ocean Eng. 31 (14–15), 1783–1834.

Davidson, D.D., Whalin, R.W., 1974. Potential Landslide-Generated Water Waves, Libby Dam and Lake Koocanusa, Montana. U.S. Army Engineer Waterways Experiment Station. Corps of Engineers, Vicksburg. Technical report H-74–15.

Dean, R.G., Dalrymple, R.A., 2004. Water wave mechanics for engineers and scientists. In: Advanced Series on Ocean Engineering, vol. 2. World Scientific, Singapore.

De Carvalho, R.F., Do Carmo, J.S.A., 2007. Landslides into reservoirs and their impacts on banks. Environ. Fluid Mech. 7, 481–493.

De Lange, S.I., Santa, N., Pudasaini, S.P., Kleinhans, M.G., de Haas, T., 2020. Debris-flow generated tsunamis and their dependence on debris-flow dynamics. Coast. Eng. 157, 103623.

Deng, B., Tao, H., Jiang, C., Qu, K., 2020. Numerical investigation on hydrodynamic characteristics of landslide-induced impulse waves in narrow river-valley reservoirs. IEEE 8, 165285–165297.

Dingemans, M.W., 1997. Water Wave Propagation over Uneven Bottoms: Part 1. World Scientific, Singapore.

Di Risio, M., Bellotti, G., Panizzo, A., De Girolamo, P., 2009a. Three-dimensional experiments on landslide generated waves at a sloping coast. Coast. Eng. 56 (5–6), 659–671.

Di Risio, M., De Girolamo, P., Bellotti, G., Panizzo, A., Aristodemo, F., Molfetta, M.G., Petril-lo, A.F., 2009b. Landslide-generated tsunamis runup at a coast of a conical island: New physical model experiments. J. Geophys. Res.-Oceans 114 (C01009).

Di Risio, M., De Girolamo, P., Beltrami, G.M., 2011. Forecasting landslide generated tsunamis: A review. In: The Tsunami Threat-research and Technology. IntechOpen.

Di Risio, M., Sammarco, P., 2008. Analytical modeling of landslide-generated impulse waves. J. Waterw. Port C.-ASCE 134 (1), 53–60.

Domínguez, J.M., Fourtakas, G., Altomare, C., Canelas, R.B., Tafuni, A., García-Feal, O., Martínez-Estévez, I., Mokos, A., Vacondio, R., Crespo, A.J.C., Rogers, B.D., Stansby, P.K., Gómez-Gesteira, M., 2022. DualSPHysics: From fluid dynamics to multiphysics problems. Comput. Part. Mech. 9 (5), 867–895. https://link.springer.com/article/10.1007/s40571-021-00404-2.

Dong, G., Wang, G., Ma, X., Ma, Y., 2010. Harbor resonance induced by subaerial landslide-generated impact waves. Ocean Eng. 37 (10), 927–934.

Evers, F.M., 2017. Spatial Propagation of Landslide Generated Impulse Waves. ETH Zurich, Zurich. Ph.D. thesis 24650.

Evers, F.M., Hager, W.H., 2015. Impulse wave generation: Comparison of free granular with mesh-packed slides. J. Mar. Sci. Eng. 3 (1), 100–110.

Evers, F.M., Hager, W.H., 2016. Spatial impulse waves: Wave height decay experiments at laboratory scale. Landslides 13, 1395–1403.

Evers, F.M., Hager, W.H., Boes, R.M., 2019a. Spatial impulse wave generation and propagation. J. Waterw. Port C.-ASCE 145 (3), 0401901–1–15.

Evers, F.M., Heller, V., Fuchs, H., Hager, W.H., Boes, R.M., 2019b. Landslide Generated Impulse Waves in Reservoirs – Basics and Computation, 2nd edition. ETH Zurich, Zurich.

Feng, X., Cheng, L., Dong, Q., Qi, X., Xiong, C., 2022. Numerical study of hydraulic characteristics of impulse waves generated by subaerial landslides. AIP Adv. 12, 121518.

Fenton, J.D., 1985. A fifth-order Stokes theory for steady waves. J. Waterw. Port, Coast. Ocean Eng. 111 (2), 216–234.

Fenton, J.D., 1999. The cnoidal theory of water waves. In: Developments in Offshore Engineering. Elsevier, pp. 55–100.

Franco, A., Schneider-Muntau, B., Roberts, N.J., Clague, J.J., Gems, B., 2021. Geometry-based preliminary quantification of landslide-induced impulse wave attenuation in mountain lakes. App. Sci.-Basel 11, 11614.

Fritz, H.M., Hager, W.H., Minor, H.-E., 2001. Lituya Bay case: Rockslide impact and wave run-up. Sci. Tsunami Hazards 19 (1), 3–22.

Fritz, H.M., Hager, W.H., Minor, H.-E., 2003. Landslide generated impulse waves. 1. Instantaneous flow fields. Exp. Fluids 35, 505–519.

Fritz, H.M., Hager, W.H., Minor, H.-E., 2003b. Landslide generated impulse waves. 2: Hydrodynamic impact craters. Exp. Fluids 35, 520–532.

Fritz, H.M., Hager, W.H., Minor, H.-E., 2004. Near field characteristics of landslide generated impulse waves. J. Waterw. Port C.-ASCE 130 (6), 287–302.

Fritz, H.M., Hillaire, J.V., Molière, E., Wei, Y., Mohammed, F., 2013. Twin tsunamis triggered by the 12 January 2010 Haiti earthquake. Pure Appl. Geophys. 170 (9–10), 1463–1474.

Fuchs, H., Boes, R., 2010. Berechnung felsrutschinduzierter Impulswellen im Vierwaldstättersee. Wasser Energie Luft 102 (3), 215–221 (in German).

Fuchs, H., Heller, V., Hager, W.H., 2010. Impulse wave run-over: Experimental benchmark study for numerical modelling. Exp. Fluids 49 (5), 985–1004.

Fuchs, H., Pfister, M., Boes, R., Perzlmaier, S., Reindl, R., 2011. Impulswellen infolge Lawineneinstoss in den Speicher Kühtai. WasserWirtschaft 101 (1–2), 54–60 (in German).

Gabl, R., Seibl, J., Gems, B., Aufleger, M., 2015. 3-D-numerical approach to simulate the overtopping volume caused by an impulse wave comparable to avalanche impact in a reservoir. Nat. Hazard. Earth Sys. 15 (12), 2617–2630.
Geertsema, M., Menounos, B., Bullard, G., Carrivick, J.L., Clague, J.J., Dai, C., Donati, D., Ekstrom, G., Jackson, J.M., Lynett, P., Pichierri, M., Pon, A., Shugar, D.H., Stead, D., Del Bel Belluz, J., Friele, P., Giesbrecht, I., Heathfield, D., Millard, T., Nasonova, S., Schaeffer, A.J., Ward, B.C., Blaney, D., Blaney, E., Brillon, C., Bunn, C., Floyd, W., Higman, B., Hughes, K.E., McInnes, W., Mukherjee, K., Sharp, M.A., 2022. The 28 November 2020 landslide, tsunami, and outburst flood – A hazard cascade associated with rapid deglaciation at Elliot Creek, British Columbia, Canada. Geophys. Res. Lett. 49 (6), e2021GL096716.
George, D.L., Iverson, R.M., Cannon, C.M., 2017. New methodology for computing tsunami generation by subaerial landslides: Application to the 2015 Tyndall Glacier landslide, Alaska. Geophys. Res. Lett. 44 (14), 7276–7284.
Géron, A., 2019. Hands-on Machine Learning with Scikit-Learn, Keras, and TensorFlow: Concepts, Tools, and Techniques to Build Intelligent Systems, 2nd ed. O'Reilly, Sebastopol, CA.
Glimsdal, S., Pedersen, G.K., Harbitz, C.B., Løvholt, F., 2013. Dispersion of tsunamis: Does it really matter? Nat. Hazard. Earth Sys. 13, 1507–1526.
Grezio, A., Babeyko, A., Baptista, M.A., Behrens, J., Costa, A., Davies, G., Geist, E.L., Glimsdal, S., González, F.I., Griffin, J., Harbitz, C.B., LeVeque, R.J., Lorito, S., Løvholt, F., Omira, R., Mueller, C., Paris, R., Parsons, T., Polet, J., Power, W., Selva, J., Sørensen, M.B., Thio, H.K., 2017. Probabilistic tsunami hazard analysis: Multiple sources and global applications. Rev. Geophys. 55, 1158–1198.
Grilli, S.T., Tappin, D.R., Carey, S., Watt, S.F.L., Ward, S.N., Grilli, A.R., Engwell, S.L., Zhang, C., Kirby, J.T., Schambach, L., Muin, M., 2019. Modelling of the tsunami from the December 22, 2018 lateral collapse of Anak Krakatau volcano in the Sunda Straits, Indonesia. Sci. Rep.-UK 9 (11046), 1–13.
Gylfadóttir, S.S., Kim, J., Helgason, J.K., Brynjólfsson, S., Höskuldsson, A., Jóhannesson, T., Harbitz, C.B., Løvholt, F., 2017. The 2014 Lake Askja rockslide induced tsunami: Optimization of numerical tsunami model using observed data. J. Geophys. Res. Oceans 122 (5), 4110–4122.
Hager, W.H., Evers, F.M., 2020. Impulse waves in reservoirs: Experimental research up to 1990. J. Hydraul. Eng. 146 (10), 03120002.
Han, L., Wang, P., Yu, T., 2022. Wave types and energy conversion of impulse waves generated by landslides into mountain reservoirs. Sci. Rep.-UK 12 (4035), 1–9.
Harbitz, C.B., Glimsdal, S., Løvholt, F., Kveldsvik, V., Pedersen, G.K., Jensen, A., 2014. Rockslide tsunamis in complex fjords: From an unstable rock slope at Åkerneset to tsunami risk in western Norway. Coast. Eng. 88, 101–122.
Heinrich, P., 1992. Nonlinear water waves generated by submarine and aerial landslides. J. Waterw. Port C.-ASCE 118 (3), 249–266.
Heller, V., 2007. Landslide Generated Impulse Waves – Prediction of near Field Characteristics. ETH Zurich, Zurich. Ph.D. thesis 17531.
Heller, V., Attili, T., Chen, F., Gabl, R., Wolters, G., 2021. Large-scale investigation into iceberg-tsunamis generated by various iceberg calving mechanisms. Coast. Eng. 163, 103745.
Heller, V., Bruggemann, M., Spinneken, J., Rogers, B., 2016. Composite modelling of subaerial landslide-tsunamis in different water body geometries and novel insight into slide and wave kinematics. Coast. Eng. 109 (3), 20–41.
Heller, V., Chen, F., Brühl, M., Gabl, R., Chen, X., Wolters, G., Fuchs, H., 2019. Large-scale experiments into the tsunamigenic potential of different iceberg calving mechanisms. Sci. Rep.-UK 9 (861), 1–10.
Heller, V., Hager, W.H., 2010. Impulse product parameter in landslide generated impulse waves. J. Waterw. Port C.-ASCE 136 (3), 145–155.
Heller, V., Hager, W.H., 2011. Wave types of landslide generated impulse waves. Ocean Eng. 38 (4), 630–640.
Heller, V., Hager, W.H., Minor, H.-E., 2008. Scale effects in subaerial landslide generated impulse waves. Exp. Fluids 44 (5), 691–703.
Heller, V., Hager, W.H., Minor, H.-E., 2009. Landslide generated impulse waves in reservoirs – Basics and computation. In: Boes, R. (Ed.), VAW Mitteilung 211. ETH Zurich, Zurich.
Heller, V., Moalemi, M., Kinnear, R.D., Adams, R.A., 2012. Geometrical effects on landslide-generated tsunamis. J. Waterw. Port C.-ASCE 138 (4), 286–298.
Heller, V., Spinneken, J., 2013. Improved landslide-tsunami predictions: Effects of block model parameters and slide model. J. Geophys. Res.-Oceans 118 (3), 1489–1507.
Heller, V., Spinneken, J., 2015. On the effect of the water body geometry on landslide-tsunamis: Physical insight from laboratory tests and 2D to 3D wave parameter transformation. Coast. Eng. 104 (10), 113–114.
Hu, Y.-X., Li, H.-B., Li, C.-J., Zhou, J.-W., 2022. Quantitative evaluation in classification and amplitude of near-field landslide generated wave induced by granular debris. Ocean Eng. 261, 112142.
Hu, Y.-X., Yu, Z.-Y., Zhou, J.-W., 2020. Numerical simulation of landslide-generated waves during the 11 October 2018 Baige landslide at the Jinsha river. Landslides 17 (10), 2317–2328.
Huang, B., Wang, S.C., Zhao, Y.B., 2017. Impulse waves in reservoirs generated by landslides into shallow water. Coast. Eng. 123, 52–61.
Huang, B., Yin, Y., Chen, X., Liu, G., Wang, S., Jiang, Z., 2014. Experimental modelling of tsunamis generated by subaerial landslides: Two case studies of the Three Gorges Reservoir, China. Environ. Earth Sci. 71 (9), 3813–3825.
Huang, B., Yin, Y., Renjiang, L., Peng, Z., Zhen, Q., Yang, L., Shulou, C., Qiuwang, L., Kaikai, X., 2023. Three-dimensional experimental investigation on hazard reduction of landslide-generated impulse waves in the Baihetan Reservoir, China. Landslides.
Huang, B., Yin, Y., Liu, G., Wang, S., Chen, X., Huo, Z., 2012. Analysis of waves generated by Gongjiafang landslide in Wu Gorge, three Gorges Reservoir, on November 23, 2008. Landslides 9 (3), 395–405.
Huang, B., Zhang, Q., Wang, J., Luo, C., Chen, X., Chen, L., 2020. Experimental study on impulse waves generated by gravitational collapse of rectangular granular piles. Phys. Fluids 32, 033301-1.
Huang, C.-S., Chan, I.-C., 2022. Effects of slide shape on impulse waves generated by a subaerial solid slide. Water 14 (17), 2643.
Huang, T.Y., Hsiao, S.C., Wu, N.J., 2013. Nonlinear wave propagation and run-up generated by subaerial landslides modeled using meshless method. Comput. Mech. 53 (2), 203–214.
Huang, Z., Law, K.T., Liu, H., Jiang, T., 2009. The chaotic characteristics of landslide evolution: A case study of Xintan landslide. Environ. Geol. 56 (8), 1585–1591.
Huber, A., 1980. Schwallwellen in Seen als Folge von Felsstürzen. ETH Zurich, Zurich Ph. D. thesis 6627 (in German). https://www.research-collection.ethz.ch/bitstream/handle/20.500.11850/136926/1/eth-35307-01.pdf.
Huber, A., Hager, W.H., 1997. Forecasting impulse waves in reservoirs. In: Proc., 19th Congrès des Grands Barrages, Florence, ICOLD, Paris, pp. 993–1005.
Hughes, S.A., 1993. Advanced series on ocean engineering 7. In: Physical Models and Laboratory Techniques in Coastal Engineering. World Scientific, London.
Iorio, V., Bellotti, G., Cecioni, C., Grilli, S.T., 2021. A numerical model for the efficient simulation of multiple landslide-induced tsunamis scenarios. Ocean Model 168 (12), 101899.
James, S.C., Zhang, Y., O'Donncha, F., 2018. A machine learning framework to forecast wave conditions. Coast. Eng. 137 (7), 1–10.
Jankaew, K., Atwater, B.F., Sawai, Y., Choowong, M., Charoentitirat, T., Martin, M.E., Prendergast, A., 2008. Medieval forewarning of the 2004 Indian Ocean tsunami in Thailand. Nature 455, 1228–1231.
Jenkins, D.G., Heller, V., Giannakidis, A., 2023. Slide type- and water body geometry-invariant learning of comprehensive subaerial landslide-tsunami characterisation. Coastal Eng. (in preparation).
Jiang, L., LeBlond, P.H., 1994. Three-dimensional modeling of tsunami generation due to a submarine mudslide. J. Phys. Oceanogr. 24 (3), 559–572.
Johnson, J.W., Bermel, K.J., 1949. Impulsive waves in shallow water as generated by falling weights. T. Am. Geophys. Un. 30 (2), 223–230.
Kajiura, K., 1963. The leading wave of tsunami. Bull. Earthq. Res. Inst. Tokyo Univ. 41 (3), 531–571.
Kamath, A., Bihs, H., Arntsen, Ø.A., 2017. Application of a 6DOF algorithm for the investigation of impulse waves generated due to sub-aerial landslides. In: MARINE 2017, VII Conference on Computational Methods in Marine Engineering, Nantes, France.
Kamphuis, J.W., Bowering, R.J., 1970. Impulse waves generated by landslides. In: Proc., 12th Coastal Engineering Conf. 1. ASCE, New York, pp. 575–588.
Kesseler, M., Heller, V., Turnbull, B., 2020. Grain Reynolds number scale effects in dry granular slides. J. Geophys. Res.-Earth 125 (1), 1–19.
Kim, D.H., Lynett, P.J., Socolofsky, S.A., 2009. A depth-integrated model for weakly dispersive, turbulent, and rotational fluid flows. Ocean Model 27 (3–4), 198–214.
Kim, J., Pedersen, G.K., Løvholt, F., LeVeque, R.J., 2017. A Boussinesq type extension of the GeoClaw model - a study of wave breaking phenomena applying dispersive long wave models. Coast. Eng. 122 (4), 75–86.
Kranzer, H.C., Keller, J.B., 1959. Water waves produced by explosions. J. Appl. Phys. 30 (3), 398–407.
Kremer, K., Anselmetti, F.S., Evers, F.M., Goff, J., Nigg, V., 2021. Freshwater (paleo) tsunamis – a review. Earth-Sci. Rev. 212, 103447.
Laitone, E.V., 1960. The second approximation to cnoidal and solitary waves. J. Fluid Mech. 9, 430–444.
Lalli, F., Postacchini, M., Brocchini, M., 2019. Long waves approaching the coast: Green's law generalization. J. Ocean Eng. Mar. Energy 5, 385–402.
Law, L., Brebner, A., 1968. On water waves generated by landslides. In: Proceedings of the Third Australasian Conference on Hydraulics and Fluid Mechanics. Inst. of Eng, Sydney, NSW, Australia, pp. 155–159.
Lee, C.-H., Huang, Z., 2022. Effects of grain size on subaerial granular landslide and resulting impulse waves: Experiment and multi-phase flow simulation. Landslides 19, 137–153.
Li, Y., Ding, Y.-N., Yang, L., Liu, X.-S., Liu, Y., 2023. A prediction model for the rockslide-generated wave amplitude under the condition of bedrock mass breakup. Ocean Eng. 272, 113845.
Lindstrøm, E.K., 2016. Waves generated by subaerial slides with various porosities. Coast. Eng. 116 (10), 170–179.
Lindstrøm, E.K., Pedersen, G.K., Jensen, A., Glimsdal, S., 2014. Experiments on slide generated waves in a 1:500 scale fjord model. Coast. Eng. 92, 12–23.
Lipiejko, N., Whittaker, C.N., Lane, E.M., White, J.D.L., Power, W.L., 2022. Experimental modeling of tsunamis generated by pyroclastic density currents: The effects of particle size distribution on wave generation. J. Geophys. Res.-Sol. Ea. 127 (11), e2022JB024847.
Liu, J., Wang, Y., Xiao, T., Yin, K., Huo, Z., Wang, X., Tang, Y., 2023a. Experimental investigation on near-field edge wave run-ups generated by landslides in narrow reservoirs. Geol. J. 1–15.
Liu, J., Wang, Y., Yin, K., Wu, L., Zhang, L., 2023b. Landslide-tsunami prediction in narrow reservoirs involving reflection. Nat. Hazards 115, 2457–2482.
Liu, P.L.-F., Lynett, P., Synolakis, C.E., 2003. Analytical solutions for forced long waves on a sloping beach. J. Fluid Mech. 478, 101–109.
Liu, P.L.-F., Wu, T.-R., Raichlen, F., Synolakis, C.E., Borrero, J.C., 2005. Runup and rundown generated by three-dimensional sliding masses. J. Fluid Mech. 536, 107–144.
Longuet-Higgins, M., 1967. On the trapping of wave energy round islands. J. Fluid Mech. 29 (4), 781–821.
Løvholt, F., Glimsdal, S., Harbitz, C.B., 2020. On the landslide tsunami uncertainty and hazard. Landslides 17, 2301–2315.

Løvholt, F., Pedersen, G., Gisler, G., 2008. Oceanic propagation of a potential tsunami from the La Palma Island. J. Geophys. Res. 113, C09026.
Lüthi, M.P., Vieli, A., 2016. Multi-method observation and analysis of a tsunami caused by glacier calving. Cryosphere 10 (3), 995–1002.
Lynett, P., Liu, L.-F., 2005. A numerical study of the run-up generated by three-dimensional landslides. J. Geophys. Res. 110, C03006.
Lynett, P.J., Borrero, J., Son, S., Wilson, R., Miller, K., 2014. Assessment of the tsunami-induced current hazard. Geophys. Res. Lett. 41 (6), 2048–2055.
Ma, G., Kirby, J.T., Hsu, T.-J., Shi, F., 2015. A two-layer granular landslide model for tsunami wave generation: Theory and computation. Ocean Model 93, 40–55.
MacFarlane, D.F., 2009. Observations and predictions of the behaviour of large, slow-moving landslides in schist, Clyde Dam reservoir, New Zealand. Eng. Geol. 109, 5–15.
Macías, J., Escalante, C., Castro, M.J., 2021. Multilayer-HySEA model validation for landslide-generated tsunamis Part 1: Rigid slides. Nat. Hazard. Earth Sys. 21 (2), 775–789.
Mazzanti, P., Bozzano, F., 2011. Revisiting the February 6th 1783 Scilla (Calabria, Italy) landslide and tsunami by numerical simulation. Mar. Geophys. Res. 32 (1–2), 273–286.
McFall, B.C., Fritz, H.M., 2016. Physical modelling of tsunamis generated by three-dimensional deformable granular landslides on planar and conical island slopes. Proc. Roy. Soc. A-Math. Phys. 472 (2188), 20160052.
McFall, B.C., Fritz, H.M., 2017. Runup of granular landslide-generated tsunamis on planar coasts and conical islands. J. Geophys. Res.-Oceans 122, 6901–6922.
Meng, Z., 2018. Experimental study on impulse waves generated by a viscoplastic material at laboratory scale. Landslides 15 (6), 1173–1182.
Meng, Z., Ancey, C., 2019. The effects of slide cohesion on impulse-wave formation. Exp. Fluids 60 (10), 151.
Meng, Z., Hu, Y., Ancey, C., 2020. Using a data driven approach to predict waves generated by gravity driven mass flows. Water 12 (2), 600.
Meyer, W., Carpenter, P.J., 1983. Filling of Spirit Lake, Washington, May 18, 1980 to July 31, 1982. US Geological Survey. Report 82-771.
Miller, G.S., Take, A.W., Mulligan, R.P., McDougall, S., 2017. Tsunamis generated by long and thin granular landslides in a large flume. J. Geophys. Res.-Oceans 122 (1), 653–668.
Mohammed, F., Fritz, H.M., 2012. Physical modeling of tsunamis generated by three-dimensional deformable granular landslides. J. Geophys. Res. 117, C11015.
Monaghan, J.J., Kos, A., 2000. Scott Russell's wave generator. Phys. Fluids 12 (3), 622–630.
Monaghan, J.J., Kos, A., Issa, N., 2003. Fluid motion generated by impact. J. Waterw. Port C.-ASCE 129 (6), 250–259.
Mu, P., Wang, P., Han, L., Wang, M., Meng, C., Cheng, Z., Xu, H., 2020. The propagation of landslide-generated impulse waves and their impacts on the moored ships: An experimental investigation. Adv. Civil Eng. 1, 1–13.
Mulligan, R.P., Franci, A., Deligueta, M.A., Take, W.A., 2020. Simulations of landslide wave generation and propagation using the particle finite element method. J. Geophys. Res.- Oceans 125 (6), e2019JC015873.
Mulligan, R.P., Take, W.A., 2017. On the transfer of momentum from a granular landslide to a water wave. Coast. Eng. 125, 16–22.
Noda, E., 1970. Water waves generated by landslides. J. Waterway. Harbour. Coast. Eng. Div. ASCE 96 (WW4), 835–855.
Osborne, A., 2010. In: Nonlinear Ocean Waves and the Inverse Scattering Transform. Elsevier, Amsterdam, p. 977.
Panizzo, A., Bellotti, G., De Girolamo, P., 2002. Application of wavelet transform analysis to landslide generated waves. Coast. Eng. 44, 321–338.
Panizzo, A., De Girolamo, P., Di Risio, M., Maistri, A., Petaccia, A., 2005a. Great landslide events in Italian artificial reservoirs. Nat. Hazard. Earth Syst. 733–740.
Panizzo, A., De Girolamo, P., Petaccia, A., 2005b. Forecasting impulse waves generated by subaerial landslides. J. Geophys. Res. 110, C12025.
Paris, R., 2015. Source mechanisms of volcanic tsunamis. Philos. T. R. Soc. A 373 (2053), 20140380.
Paris, R., Bravo, J.J.C., González, M.E.M., Kelfoun, K., Nauret, F., 2017. Explosive eruption, flank collapse and megatsunami at Tenerife ca. 170 ka. Nat. Commun. 8 (1), 1–8, 15246.
Paris, A., Okal, E.A., Guérin, C., Heinrich, P., Schindelé, F., Hébert, H., 2019. Numerical modeling of the June 17, 2017 landslide and tsunami events in Karrat Fjord, West Greenland. Pure Appl. Geophys. 176, 3035–3057.
Qiu, L.-C., Tian, L., Liu, X.-J., Han, Y., 2019. A 3D multiple-relaxation-time LBM for modeling landslide-induced tsunami waves. Eng. Anal. Bound. Elem. 102 (5), 51–59.
Rauter, M., Hoße, L., Mulligan, R.P., Take, W.A., Løvholt, F., 2021. Numerical simulation of impulse wave generation by idealized landslides with OpenFOAM. Coast. Eng. 165, 103815.
Rauter, M., Viroulet, S., Gylfadóttir, S.S., Fellin, W., Løvholt, F., 2022. Granular porous landslide tsunami modelling - the 2014 Lake Askja flank collapse. Nat. Commun. 13 (678), 1–13.
Renzi, E., Sammarco, P., 2010. Landslide tsunamis propagating around a conical island. J. Fluid Mech. 650, 251–285.
Renzi, E., Sammarco, P., 2012. The influence of landslide shape and continental shelf on landslide generated tsunamis along a plane beach. Nat. Hazards Earth Syst. Sci. 12, 1503–1520.
Robbe-Saule, M., Morize, C., Henaff, R., Bertho, Y., Sauret, A., Gondret, P., 2021. Experimental investigation of tsunami waves generated by granular collapse into water. J. Fluid Mech. 907, A11.
Roberts, N.J., McKillop, R., Hermanns, R.L., Clague, J.J., Oppikofer, T., 2014. Preliminary global catalogue of displacement waves from subaerial landslides. In: Landslide Science for a Safer Geoenvironment. Springer, Cham, pp. 687–692.
Romano, A., 2020. Physical and Numerical Modeling of Landslide-Generated Tsunamis: A Review. In: Geophysics and Ocean Wave Studies. IntechOpen. https://doi.org/10.5772/intechopen.93878. Chapter 8.
Romano, A., Bellotti, G., Di Risio, M., 2013. Wavenumber–frequency analysis of the landslide-generated tsunamis at a conical island. Coast. Eng. 81, 32–43.
Romano, A., Di Risio, M., Bellotti, G., Molfetta, M.G., Damiani, L., De Girolamo, P., 2016. Tsunamis generated by landslides at the coast of conical islands: Experimental benchmark dataset for mathematical model validation. Landslides 13 (6), 1379–1393.
Ruffini, G., Heller, V., Briganti, R., 2019. Numerical modelling of landslide-tsunami propagation in a wide range of idealised water body geometries. Coast. Eng. 153, 103518.
Ruffini, G., Heller, V., Briganti, R., 2021. Numerical characterisation and efficient prediction of landslide-tsunami propagation over a wide range of idealised bathymetries. Coast. Eng. 167, 103854.
Russell, J.S., 1837. Report of the committee on waves. In: 7th Meeting of the British Association for the Advancement of Science. Liverpool, UK, pp. 417–496.
Sabeti, R., Heidarzadeh, M., 2022. Numerical simulations of water waves generated by subaerial granular and solid-block landslides: Validation, comparison, and predictive equations. Ocean Eng. 266 (3), 112853.
Sælevik, G., Jensen, A., Pedersen, G., 2009. Experimental investigation of impact generated tsunami; related to a potential rock slide, Western Norway. Coast. Eng. 56 (9), 897–906.
Sammarco, P., Renzi, E., 2008. Landslide tsunamis propagating along a plane beach. J. Fluid Mech. 598, 107–119.
Sarlin, W., Morize, C., Sauret, A., Gondret, P., 2021. Nonlinear regimes of tsunami waves generated by a granular collapse. J. Fluid Mech. 919, R6.
Satake, K., 2007. Volcanic origin of the 1741 Oshima-Oshima tsunami in the Japan Sea. Earth Planets Space 59 (5), 381–390.
Sauter, E., Fuchs, H., Schmocker, L., Volkwein, A., Prohaska, Y., Boes, R.M., 2019. Large-scale field tests on impulse waves. In: Proc. 38th IAHR World Congress, pp. 727–739.
Shan, T., Zhao, J., 2014. A coupled CFD-DEM analysis of granular flow impacting on a water reservoir. Acta Mech. 225, 2449–2470.
Shi, F., Kirby, J.T., Harris, J.C., Geiman, J.D., Grilli, S.T., 2012. A high-order adaptive time-stepping TVD solver for Boussinesq modeling of breaking waves and coastal inundation. Ocean Model 43, 36–51.
Slingerland, R.L., Voight, B., 1979. Occurrences, properties and predictive models of landslide-generated impulse waves. In: Voight, B. (Ed.), Rockslides and Avalanches 2. Elsevier, Amsterdam, pp. 317–397.
Slingerland, R.L., Voight, B., 1982. Evaluating hazard of landslide-induced water waves. J. Waterw. Port C.-ASCE 108 (WW4), 504–512.
Smith, R.C., Hill, J., Collins, G.S., Piggott, M.D., Kramer, S.C., Parkinson, S.D., Wilson, C., 2016. Comparing approaches for numerical modelling of tsunami generation by deformable submarine slides. Ocean Model 100 (4), 125–140.
Synolakis, C.E., Skjelbreia, J.E., 1993. Evolution of maximum amplitude of solitary waves on plane beaches. J. Waterw. Port C.-ASCE 119 (3), 323–342.
Takabatake, T., Mäll, M., Han, D.C., Inagaki, N., Kisizaki, D., Esteban, M., Shibayama, T., 2020. Physical modelling of tsunamis generated by subaerial, partially submerged, and submarine landslides. Coast. Eng. J. 62 (4), 582–601.
Tan, H., Ruffini, G., Chen, S., Heller, V., 2018. A numerical landslide-tsunami hazard assessment technique applied on hypothetical scenarios at Es Vedrà, offshore Ibiza. J. Mar. Sci. Eng. 6 (4), 1–22.
Tanaka, M., 1986. The stability of solitary waves. Phys. Fluids 29, 650–655.
Tang, G., Lu, L., Teng, Y., Zhang, Z., Xie, Z., 2018. Impulse waves generated by subaerial landslides of combined block mass and granular material. Coast. Eng. 141 (11), 68–85.
Tehranirad, B., Harris, J.C., Grilli, A.R., Grilli, S.T., Abadie, S., Kirby, J.T., Shi, F., 2015. Far-field tsunami impact in the North Atlantic basin from large scale flank collapses of the Cumbre Vieja volcano, La Palma. Pure Appl. Geophys. 172, 3589–3616.
Tessema, N.N., Sigtryggsdóttir, F.G., Lia, L., Jabir, A.K., 2019. Case study of dam overtopping from waves generated by landslides impinging perpendicular to a reservoir's longitudinal axis. J. Mar. Sci. Eng. 7 (7), 221.
Tinti, S., Pagnoni, G., Zaniboni, F., 2006. The landslides and tsunamis of the 30th of December 2002 in Stromboli analysed through numerical simulations. Bull. Volcanol. 68 (5), 462–479.
Ursell, F., 1952. Edge waves on a sloping beach. P. Roy. Soc. A-Math. Phy. 214, 79–97.
Ursell, F., 1953. The long-wave paradox in the theory of gravity waves. P. Camb. Philos. Soc. 49, 685–694.
Van der Meer, J.W., Briganti, R., Zanuttigh, B., Wang, B., 2005. Wave transmission and reflection at low-crested structures: Design formulae, oblique wave attack and spectral change. Coast. Eng. 52 (10), 915–929.
Violeau, D., Rogers, B.D., 2016. Smoothed particle hydrodynamics (SPH) for free-surface flows: Past, present and future. J. Hydraul. Res. 54 (1), 1–26.
Viroulet, S., Cébron, D., Kimmoun, O., Kharif, C., 2013a. Shallow water waves generated by subaerial solid landslides. Geophys. J. Int. 193 (2), 747–762.
Viroulet, S., Sauret, A., Kimmoun, O., 2014. Tsunami generated by a granular collapse down a rough inclined plane. EPL 105 (34), 004.
Viroulet, S., Sauret, A., Kimmoun, O., Kharif, C., 2013b. Granular collapse into water: Toward tsunami landslides. J. Visual.-Jpn. 16 (3), 189–191.
Voight, B., Janda, R.J., Glicken, H., Douglass, P.M., 1983. Nature and mechanics of the Mount St Helens rockslide-avalanche of 18 May 1980. Géotechnique 33 (3), 243–273.
Walder, J.S., Watts, P., Sorensen, O.E., Janssen, K., 2003. Tsunamis generated by subaerial mass flows. J. Geophys. Res. 108 (B5), 2236 (2).
Waldmann, N., Vasskog, K., Simpson, G., Chapron, E., Støren, E.W.N., Hansen, L., Loizeau, J.-L., Nesje, A., Ariztegui, D., 2021. Anatomy of a catastrophe:

Reconstructing the 1936 rock fall and tsunami event in lake Lovatnet, Western Norway. Front. Earth Sci. 9, 364.
Wang, B., Yao, L., Zhao, H., Zhang, C., 2018. The maximum height and attenuation of impulse waves generated by subaerial landslides. Shock. Vib. 2018, 1–14.
Wang, J., Ward, S.N., Xiao, L., 2015. Numerical simulation of the December 4, 2007 landslide-generated tsunami in Chehalis, Lake Canada. Geophys. J. Int. 201 (1), 372–376.
Wang, J., Ward, S.N., Xiao, L., 2019a. Tsunami Squares modeling of landslide generated impulsive waves and its application to the 1792 Unzen-Mayuyama mega-slide in Japan. Eng. Geol. 256, 121–137.
Wang, R., Wang, Y., Wan, J., Xu, W., Yang, Y., Wang, H., 2023. Propagation mechanism of deep-water impulse waves generated by landslides in V-shaped river channels of mountain valleys: Physical model of regular rigid block. Geofluids 1743305, 1–15.
Wang, W., Chen, G., Yin, K., Wang, Y., Zhou, S., Liu, Y., 2016. Modeling of landslide generated impulse waves considering complex topography in reservoir area. Environ. Earth Sci. 75, 1–15.
Wang, Y., Liu, J., Li, D., Yan, S., 2017. Optimization model for maximum tsunami amplitude generated by riverfront landslides based on laboratory investigations. Ocean Eng. 142, 433–440.
Wang, Y., Liu, J., Yin, K., Yu, L., Zhou, H., Hou, Z., 2019b. Comparison between the first and second wave crest amplitude generated by landslides. Ocean Eng. 171, 71–77.
Ward, S.N., Asphaug, E., 2003. Asteroid impact tsunami in 2880 March 16. Geophys. J. Int. 153, F6–F10.
Ward, S.N., Day, S., 2003. Ritter island volcano – Lateral collapse and the tsunami of 1888. Geophys. J. Int. 154 (3), 891–902.
Watt, S.F.L., Talling, P.J., Vardy, M.E., Heller, V., Hühnerbach, V., Urlaub, M., Sarkar, S., Masson, D.G., Henstock, T.J., Minshull, T.A., Paulatto, M., Le Friant, A., Lebas, E., Berndt, C., Crutchley, G.J., Karstens, J., Stinton, A.J., Maeno, F., 2012. Combinations of volcanic-flank and seafloor-sediment failure offshore Montserrat, and their implications for tsunami generation. Earth Planet. Sci. Lett. 319–320, 228–240.
WCHL, 1970. Hydraulic model studies – Wave action generated by slides into Mica Reservoir – British Columbia. Western Canada Hydraulic Laboratories, Vancouver. Report.
Wiegel, R.L., Noda, E.K., Kuba, E.M., Gee, D.M., Tornberg, G.F., 1970. Water waves generated by landslides in reservoirs. J. Waterway Harbour. Coast. Eng. Div. ASCE 96 (WW2), 307–333.
Winckler, P., Liu, P.L.F., 2015. Long waves in a straight channel with non uniform cross-section. J. Fluid Mech. 770, 156–188.
Wu, Y., Shao, K., Piccialli, F., Mei, G., 2022. Numerical modeling of the propagation process of landslide surge using physics-informed deep learning. Adv. Model. Simul. Eng. Sci. 9, 14.
Wüthrich, D., Pfister, M., Nistor, I., Schleiss, A.J., 2018. Experimental study on forces exerted on buildings with openings due to extreme hydrodynamic events. Coast. Eng. 140, 72–86.
Xiao, L., Wang, J., Ward, S.N., Chen, L., 2018. Numerical modeling of the June 24, 2015, Hongyanzi landslide generated impulse waves in Three Gorges Reservoir, China. Landslides 15 (12), 2385–2398.
Xing, A., Xu, Q., Zhu, Y., Zhu, J., Jiang, Y., 2016. The August 27, 2014, rock avalanche and related impulse water waves in Fuquan, Guizhou, China. Landslides 13 (2), 411–422.
Xue, H., Ma, Q., Diao, M., Jiang, L., 2019. Propagation characteristics of subaerial landslide-generated impulse waves. Environ. Fluid Mech. 19 (1), 203–230.
Yavari-Ramshe, S., Ataie-Ashtiani, B., 2016. Numerical modelling of subaerial and submarine landslide-generated tsunami waves - recent advances and future challenges. Landslides 13 (6), 1325–1368.
Yavari-Ramshe, S., Ataie-Ashtiani, B., 2019. On the effects of landslide deformability and initial sub-mergence on landslide-generated waves. Landslides 16 (1), 37–53.
Yin, Y.-P., Huang, B., Chen, X., Liu, G., Wang, S., 2015. Numerical analysis on wave generated by the Qianjiangping landslide in Three Gorges Reservoir, China. Landslides 12 (2), 355–364.
Zhang, Y., Li, D., Yin, K., Xiao, L., Fu, X., Glade, T., Leo, C., 2020. Numerical analysis of landslide-generated impulse waves affected by the reservoir geometry. Eng. Geol. 266 (3), 10530.
Zhao, H., Yao, L., 2019. Model tests for surge height of rock avalanche-debris flows based on momentum balance. J. Mod. Transport. 27 (4), 334–340.
Zijlema, M., Stelling, G., Smit, P., 2011. SWASH: An operational public domain code for simulating wave fields and rapidly varied flows in coastal waters. Coast. Eng. 58 (10), 992–1012.
Zitti, G., Ancey, C., Postacchini, M., Brocchini, M., 2016. Impulse waves generated by snow avalanches: Momentum and energy transfer to a water body. J. Geophys. Res.-Earth 121 (12), 2399–2423.
Zweifel, A., 2004. Impulswellen: Effekte der Rutschdichte und der Wassertiefe. ETH Zurich, Zurich. Ph.D. thesis 15596.
Zweifel, A., Hager, W.H., Minor, H.-E., 2006. Plane impulse waves in reservoirs. J. Waterw. Port C.-ASCE 132 (5), 358–368.